

Table of Contents

EXECUTIVE SUMMARY.....	1
Overview of STS-81 Mir Photo/TV Survey.....	1
Summary of Findings.....	2
1. OVERVIEW OF ANALYSES.....	4
1.1 Mir Configuration.....	4
1.2 Mir Surface Assessment.....	5
1.3 Docking Mechanism Assessment.....	5
1.4 Solar Array Motion Analysis from Video.....	5
1.5 Debris During Docking Operations.....	6
1.6 Mir Environmental Effects Payload Experiments.....	6
1.7 Alignment of ODS Centerline Video Camera.....	6
1.8 Position of the New Kurs Antenna Attached to the Docking Module.....	7
1.9 Imagery Evaluation.....	7
2. MIR CONFIGURATION.....	8
3. MIR SURFACE ASSESSMENT.....	15
4. DOCKING MECHANISM ASSESSMENT.....	35
5. MIR STRUCTURAL DYNAMICS EXPERIMENT SOLAR ARRAY MOTION.....	38
5.1 Solar Array Video Data Acquisition.....	38
5.2 Data Analysis Approach.....	40
5.3 Results: Motion Analysis of Kvant-2 Solar Panel #2.....	41
5.4 Recommendations.....	41
6. DEBRIS DURING DOCKING OPERATIONS.....	44
7. MIR ENVIRONMENTAL EFFECTS PAYLOAD ASSESSMENT.....	48
8. CENTERLINE CAMERA ALIGNMENT.....	51
8.1 Determination of Position and Roll of Centerline Camera Relative to the ODS.....	52
8.2 Determination of Indicated Roll of the Centerline Camera.....	53
8.3 Results.....	55
9. POSITION OF THE NEW KURS ANTENNA ATTACHED TO THE DOCKING MODULE.....	57
10. IMAGERY EVALUATION.....	60
10.1 Video Review.....	60
10.2 Still Photography Review.....	61
10.3 Evaluation of 400 mm lens.....	62
11. CONCLUSIONS AND RECOMMENDATIONS.....	63
11.1 Summary.....	63
11.2 Conclusions.....	64
11.3 Recommendations.....	64
12. REFERENCES.....	66

Table of Contents

13. ACRONYMS & ABBREVIATIONS.....	67
--	-----------

Table of Contents

APPENDICES

- Appendix A: Electrical Connector Report**
- Appendix B: STS-81 Mir Surface Damage and Discoloration**
- Appendix C: STS-81 Film Scenelist**
- Appendix D: STS-81 Video Scenelist**
- Appendix E: Sources for Report Imagery**
- Appendix F: STS-81 Camera Layout**

List of Figures

Figure 1.1	Mir Space Station.....	4
Figure 2.1	Docking Module / Kristall.....	8
Figure 2.2	Docking Module / Orbiter Docking System (ODS).....	9
Figure 2.3	Priroda.....	10
Figure 2.4	Spektr.....	11
Figure 2.5	Base Block.....	12
Figure 2.6	Kvant.....	13
Figure 2.7	Docking Node.....	14
Figure 3.1a	Mir Base Block - Luch antenna.....	16
Figure 3.1b	Mir Base Block - Thruster Engines and Optical Window.....	17
Figure 3.2a	Kvant - Aft Facing Section of the Module in the -YB Direction.....	18
Figure 3.2b	Kvant - Docked Section Aft of the Base Block in the -ZB Direction.....	19
Figure 3.3a	Kristall - Buran TV Target and Thruster Engines in the -XB Direction	20
Figure 3.3b	Kristall - Mooring and Stabilization Engines in the -XB Direction.....	21
Figure 3.3c	Kristall - Iгла Antenna Cable Mechanism in the -XB Direction.....	22
Figure 3.4a	Docking Module - ROEU-PDA.....	23
Figure 3.4b	Docking Module - HARR	24
Figure 3.4c	Docking Module - RSA.....	25
Figure 3.4d	Docking Module - Comparison of RSA: STS-76 vs STS-81	26
Figure 3.5a	Spektr - Solar Array Attach Point: SP#2.....	27
Figure 3.5b	Spektr - Thruster Engines	28
Figure 3.5c	Spektr - Thruster Engines and Thermal Blankets.....	29
Figure 3.5d	Spektr - Comparison of a Possible Radiator Leak: STS-79 vs STS-81.....	30
Figure 3.6	Kvant-2 - MSRE.....	31
Figure 3.7	Priroda as seen from the -XB Direction.....	32
Figure 3.8a	Kvant-2 - Solar Array: SP#2.....	33
Figure 3.8b	Base Block - Solar Array.....	34
Figure 4.1	Photo of Docking Mechanism during Approach.....	35
Figure 4.2	Enhanced Image Showing Discoloration and Shielded Strip on Non-Axial Target Backplate.....	36
Figure 4.3	Composite Image of Docking Mechanism during Approach.....	37
Figure 4.4	Image of Portion of Docking Mechanism during Backaway.....	37
Figure 5.1	A Muxed Video Frame Used in Motion Analysis of Kvant-2 SP#2.....	39
Figure 5.2	An Example of Acceptable (left) and Unacceptable (Pixel Shifted) Video Frames.....	40
Figure 5.3	Out-Of-Plane Deflection of Kvant-2 SP#2	42
Figure 5.4	In-Plane Deflection of Kvant-2 SP#2.....	42
Figure 5.5	Fourier Transform Results for Out-of-Plane Deflection for Kvant-2 SP#2 ..	43
Figure 5.6	Fourier Transform Results for In-Plane Deflection of Kvant-2 SP#2.....	43
Figure 6.1	Trajectories of Small Debris Observed during Soft Dock.....	44
Figure 6.2	Debris Observed in Payload Bay Area during Soft Dock.....	45
Figure 6.3	Debris Observed Internal to ODS during Soft Dock.....	46
Figure 6.4	Apparent Debris Impact and Disintegration.....	46
Figure 7.1	STS-81 Image of Mir with MEEP Experiments	48
Figure 7.2	Video Image of POSA Front Panel.....	49
Figure 7.3	Still Photographs of POSA II Front and Back Panels.....	50
Figure 7.4	Still Photographs of POSA, PPMD, and ODC Back Panels.....	50
Figure 8.1	Stand-off Target and Backplate.....	51
Figure 8.2	ODS Features Used in Alignment Analysis	52
Figure 8.3	The Relative Centers of the ODS as Computed from the Alignment Guides, the Video Frame, and the Alignment Washers.....	54
Figure 9.1	Kurs Antenna as seen from the Shuttle Flight Deck on STS-81.....	57
Figure 9.2	Kurs Antenna as seen from Payload Bay Camera A	58
Figure 9.3	Kurs Antenna as seen from Payload Bay Camera D	59

List of Tables

Table 8-1	Analysis Cases and Video Availability.....	52
Table 8-2	Camera Indicated Roll Relative to Mir	55

EXECUTIVE SUMMARY

NASA and the Russian Space Agency (RSA) are involved in a cooperative venture in which the Shuttle will rendezvous and dock with the Mir Space Station during several missions from 1995 to 1998. This sequence of nine missions will serve as a precursor to the two nations' involvement in the International Space Station. These joint missions provide NASA scientists and engineers an opportunity to study the orbital, dynamic, and environmental conditions of long duration spacecraft, as well as develop evaluation and risk mitigation techniques which have direct application to the International Space Station.

Shuttle mission STS-81, launched on January 12, 1997, was docked to the Mir Space Station from January 15 through January 20, 1997. This was the Shuttle's sixth rendezvous mission with, and fifth docking to, the Mir Space Station.

Detailed Test Objective 1118 (DTO-1118) integrates the requirements for photographic and video imagery of the Mir Space Station generated by the engineering, operations, and science communities within NASA. Although mission requirements vary, the principal objectives of the DTO-1118 Mir Photo/TV Surveys are as follows:

- Study the effects of the space environment on a long-duration orbiting platform.
- Assess the overall condition of the Mir.
- Provide assurance of crew and Shuttle safety while in the proximity of the Mir Space Station.
- Analyze the dynamic effects of structures and appendages (e.g., solar array motion).
- Understand the impact of plume impingement during proximity operations.
- Evaluate the equipment and procedures used to gather survey data.

This report documents the results from STS-81 survey-related imagery analysis tasks. Reports of previous Mir surveys are listed in Section 12, References.

Overview of STS-81 Mir Photo/TV Survey

As part of DTO-1118, approximately 912 photographs and 18 hours of video of the Mir Space Station were acquired during the STS-81 mission.

The Image Science & Analysis Group (IS&AG) conducted several analysis tasks (based on user requirements) using the imagery data from STS-81. These analysis tasks were to:

- Verify the configuration of the Mir complex.
- Assess the effect of micrometeoroid impacts and other visible damage on Mir surfaces.
- Compare the condition of Station external surfaces to that seen on previous missions.
- Measure the motion of the Mir Base Block SP#2 in response to prescribed firings of Shuttle thrusters while the Shuttle was docked to Mir.
- Measure the motion of Kvant-2 SP#2 in response to prescribed firings of Mir thrusters while the Shuttle was docked to Mir.
- Document the condition of the docking mechanism.
- Characterize debris seen during and after docking operations.
- Evaluate imagery for potential contamination of the electrical connectors on the Mir docking mechanism.
- Evaluate the alignment of the Shuttle Orbiter Docking System (ODS) centerline video camera.

-
- Determine the position of the new Kurs antenna attached to the Mir Docking Module (DM) in relation to the Shuttle for potential clearance issues on the subsequent STS-91 docking mission.
 - Assess the quality of video and photographic data.

Summary of Findings

This mission report contains the results of analyses of still photography and video from STS-81. The significant findings from this mission are as follows:

- A possible leak was discovered on the Spektr radiator. The leak existed on STS-76 and STS-79, but was small and went undetected. The area is still small (approximately 7 sq. cm.), but has significantly increased in size since STS-79. See Section 3.
- Charring and probable burn-throughs were found in the protective casing of the Iгла antenna cable attached to Kristall. See Section 3.
- Additional paint was missing on the Spektr radiator as compared to that identified in the STS-79 mission report. See Section 3.
- Additional areas of peeled paint were found on the upper side of the Reusable Solar Array (RSA) carrier. During STS-79, large areas of paint were identified as peeling on the lower side of the RSA. See Section 3.
- Discolorations were found around the rivets of Base Block and inside the Kristall thruster nozzle, and color patterns similar to interference patterns of reflected light were noted on metallic surfaces of Kristall and Spektr. Details of large areas of discoloration on Base Block, Kvant, Kristall, Kvant-2, Spektr, Priroda, and the Docking Module were characterized. See Section 3.
- All capture and structural latches of the Mir Docking Module docking mechanism were found to be in good condition and in proper position before docking and after separation. All laser retroreflectors and electrical connectors were observed to be in good physical condition. See Section 4.
- Discoloration on the non-axial docking target of the Mir Docking Module was characterized. Traces of discoloration indicative of contamination were also found near the structural latches of the docking mechanism, however the traces did not extend to the laser retroreflectors or the electrical connectors. See Section 4.
- A study was conducted of possible contamination on the docking mechanism electrical connectors. However no conclusive results were obtained. Recommendations were made for further imagery acquisition and analyses. See Appendix A.
- Analyses of solar array motion from Shuttle PLB video cameras were performed in support of the Mir Structural Dynamics Experiment (MiSDE). Measurements were made of the motion of Kvant-2 SP#2 in response to one Mir thruster firing sequence. The peak-to-peak deflections were approximately 1.3 inches in out-of-plane motion and 2.2 inches for in-plane motion. The dominant frequency for both the in-plane and out-of-plane motions was 0.4 Hz. The structural model predicted frequencies at approximately 0.15 and 0.4 Hz. Additional analyses are being performed on video of Base Block SP#2 motion in response to Shuttle thruster firing sequences. Video for two of the five Base Block SP#2 test cases was not acquired because camera set-up was not completed before the thruster firings had begun. Also, the video data could not be precisely correlated to the Mir and Shuttle thruster firings because required timing data was not recorded on the video. A description of the issues, analyses, and results are provided in Section 5.
- Only small debris was observed during approach and docking. Two pieces appeared to contact camera lenses. There was no indicated debris damage. See Section 6.

-
- No damage or discoloration was observed on the Mir Environmental Effects Payload (MEEP) experiment front panels. First time imagery was obtained of the back panels on MEEP experiments. See Section 7.
 - The Shuttle crew observed an indicated yaw of the Shuttle relative to Mir during docking. Post-mission imagery analysis measured the indicated alignment of the Orbiter Docking System (ODS) centerline camera during docking and pre-separation. Both positional and rotational misalignments of the ODS centerline camera were indicated. Comparisons were also made of indicated misalignments in roll of the centerline and non-axial cameras relative to the Mir docking targets. See Section 8.
 - The Shuttle coordinates for the tip of the new Kurs antenna were determined to support calculations of the projected clearance of the antenna from the Shuttle forward bulkhead for the planned STS-91 mission to be launched in May 1998. This Kurs antenna is attached to the Mir Docking Module, and the ODS will be located closer to the forward bulkhead on STS-91. The clearance between the tip of the antenna and the forward bulkhead on STS-81 was 109 inches. See Section 9.
 - The utility of the Nikon 35 mm camera with the 400 mm lens was validated for DTO-1118 imagery acquisition. A recommendation is made for this camera and lens combination to be the primary photographic equipment for high-resolution survey imagery acquisition. See Sections 2, 3, 4, 7, and 10.

Additional conclusions and recommendations are included as Section 11 of this Mission Report.

1. OVERVIEW OF ANALYSES

1.1 Mir Configuration

The configuration of the Mir Space Station for STS-81 was essentially the same as it was for STS-79. New additions to Mir were a Kurs antenna attached to the Docking Module and a power cable on the Base Block module. The power cable extends from the attach point of the Base Block SP#3 to the Cooperative Solar Array (CSA).

Information on the Mir configuration is important for proximity operations requiring visual navigation and for conducting simulations of structural loads on docked configurations. Available drawings of the Mir Space Station were compared to photography acquired during the rendezvous. The fly-around view in Figure 1.1 identifies different Mir modules photographed during STS-81. Annotated images of the individual modules are provided in Section 2.

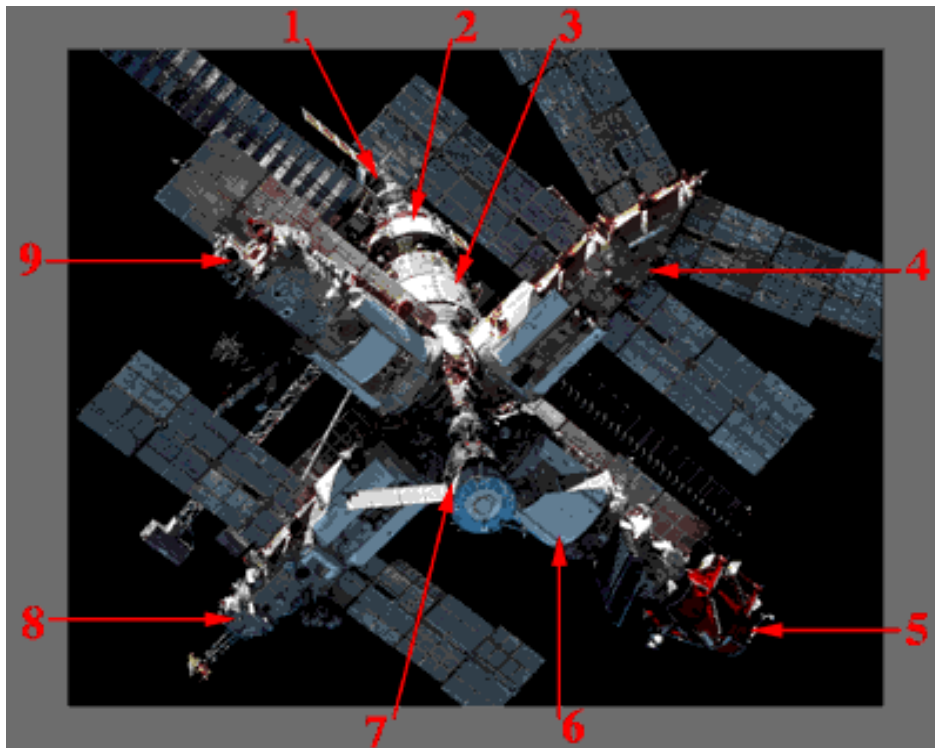


Figure 1.1 Mir Space Station

- | | |
|-------------------|-------------|
| 1. Progress | 6. Kristall |
| 2. Kvant | 7. Soyuz |
| 3. Base Block | 8. Kvant-2 |
| 4. Spektr | 9. Priroda |
| 5. Docking Module | |

1.2 Mir Surface Assessment

The purpose of surface assessment is to document the effects of the space environment on Mir Space Station materials. Three categories of surface assessments are identified: (1) anomalies identified for the first time, (2) changes in surface condition from previous missions, and (3) surface conditions where STS-81 provided improved detail over previous missions.

Anomalies identified were a possible leak in the Spektr radiator, probable burn-throughs in the protective covering of a cable to the Iгла antenna attached to Kristall, apparent depositions in the interior of the Kristall thruster nozzles, thermal blankets on Spektr which appear to be charred, and discolorations on metallic surfaces. In addition, there are probable micrometeoroid/orbital debris penetrations of the Kvant-2 SP#2 solar array.

Changes included additional paint peeling on the Spektr radiator and the upper side of the Reusable Solar Array (RSA) carrier. Additional details of paint blistering and peeling, discolorations, and damage to solar panels are noted.

Imagery and descriptions are provided in Section 3 and in Appendix B.

1.3 Docking Mechanism Assessment

An overall assessment of the docking mechanism and its visible targets is made on each docking mission. Imagery of the docking mechanism was acquired with the 35 mm camera during approach and backaway, with the ODS centerline and non-axial video cameras during approach and backaway, and with payload bay video cameras during approach and backaway. The best imagery obtained to date of the docking mechanism was captured with the 35 mm camera at close range during both docking and backaway. These images showed the centerline target, repaired on STS-79, to be in good condition for docking. All capture and structural latches were in proper position and there were no indicated issues with the laser retroreflectors and electrical connectors. Some discoloration was noted on the non-axial target and traces of possible discoloration appeared adjacent to the docking latches. Imagery and analyses are provided in Section 4. At the request of the Independent Assessment Office, an analysis was made of possible discoloration of the electrical connectors. The results of this study are included as Appendix A of this report.

1.4 Solar Array Motion Analysis from Video

The Mir Structural Dynamics Experiment (MiSDE) was performed on STS-81. Acquisition procedures were developed to obtain data and perform analyses of the motion of Kvant-2 SP#2 during a single thruster firing sequence from the Mir and the motion of Base Block SP#2 during five controlled thruster firing sequences from the Shuttle. However, several problems were experienced in the acquisition of the required video data of the solar arrays:

- a. The allocated time for the crew to perform the set-up of the cameras occurred during night passes and the crew could not see sufficient detail in the video image to align the cameras and optimize the solar arrays in the camera field-of-view. In the case of Base Block SP#2, the camera set-up could not be completed until the beginning of the daylight pass. Unfortunately, the Shuttle thruster firing sequence had already begun. As a result, video was not acquired for two of the five thruster firing sequences.
- b. To correlate solar array motion with thruster firings and accelerometer data, and to correlate tip and attach point motions, it is necessary to have IRIG timing

recorded onto the tapes which contain the MiSDE video. However, synchronous timing was not obtained.

- c. A smudge was present on the center of the lens of camera A. This smudge caused a permanent glare, and reductions in contrast in the smudged region were present in all MiSDE video utilizing camera A. As a result, automated techniques (line-tracking and point-tracking) did not provide reliable results on the position of the tip of the array from frame-to-frame and data was extracted manually.

The Mir thruster firing video was the first sequence selected for analysis. Thirty seconds of video of the solar array motion was selected for analysis of the array motion. The peak-to-peak deflections were approximately 1.3 inches of out-of-plane motion and 2.2 inches of in-plane motion. The dominant frequency for both the in-plane and out-of-plane motions was approximately 0.4 Hz. The structural model predicted frequencies at approximately 0.15 and 0.4 Hz. Video analyses of the motion of Base Block SP#2 have been initiated but are not completed. A description of the issues, analyses, and results are provided in Section 5.

Shuttle docking was also a source of solar array motion on the Mir. The CSA exhibits in- and out-of-plane motion when perturbed by the docking of the Shuttle. This was imaged from PLB Camera B, however, analysis of the motion was not feasible due to the image quality and wide field-of-view of Camera B. Camera B was the Intensified Television Camera (ITVC).

1.5 Debris During Docking Operations

No large pieces of debris were observed on STS-81. Small pieces of debris were seen during approach and docking, primarily around the time of first contact and soft dock. PLB Camera D showed small pieces of debris which originated from the Shuttle payload bay and move in the Shuttle +Z direction. Debris was also observed to originate from near the DM/ODS interface and traverse in a direction orthogonal to the DM with a small +Z component. No debris was observed to contact Mir. One piece of debris was observed moving in a direction which would indicate it may have originated from Mir. Small debris was also observed within the ODS. One small piece of debris was shown to adhere to the lens front of the PLB Camera A. Another piece of debris apparently impacts the lens of the centerline camera and disintegrates. Imagery and descriptions are provided in Section 6.

1.6 Mir Environmental Effects Payload Experiments

The Mir Environmental Effects Payload (MEEP) experiments were deployed on the exterior of the Docking Module during STS-76. Imagery of the MEEP experiments is collected on each Shuttle/Mir mission and analyzed for changes. Previous Shuttle/Mir missions provided imagery of the MEEP panels on the side oriented toward the cameras of the docked Shuttle. During STS-81, imagery was also obtained of the "back-side" panels facing the Mir. This imagery was obtained during the Shuttle fly-around. There are no indicated changes to the MEEP experiments since they were deployed. The imagery is shown in Section 7.

1.7 Alignment of ODS Centerline Video Camera

During STS-81 docking procedures, a perceived Shuttle yaw error relative to Mir was measured with the ODS centerline camera. The Orbiter yaw was changed and docking proceeded normally. The JSC Structures and Dynamics Division requested an analysis of centerline camera video recorded during docking to determine if the error was due to the alignment of the centerline camera in relation to the ODS. The imagery analysis indicated

the camera was rotated about its optical axis and not centered in the ODS. Additionally, the indicated roll of the centerline camera was determined prior to docking, at soft dock, and prior to separation. The analysis of this video is presented in Section 8.

1.8 Position of the New Kurs Antenna Attached to the Docking Module

At the request of the JSC Structures and Mechanics Division, video imagery was used to determine the position of the newly-installed Kurs antenna attached to the Mir Docking Module. The Kurs antenna currently extends toward the Shuttle Payload Bay forward bulkhead. The location of the antenna tip in Shuttle Structural Coordinates during STS-81 is $X_O = 685.5 \pm 1.9$, $Y_O = 42.3 \pm 1.1$, $Z_O = 439.3 \pm 0.9$ inches. The expected coordinates based on data obtained from the Space Shuttle Program Integration Engineering Office are $X_O = 683.4$ inches, $Y_O = 40.5$ inches, $Z_O = 439.1$ inches. Analyses are described in Section 9.

1.9 Imagery Evaluation

The coverage and quality of the still photography was the best obtained to date for DTO-1118. Surveys obtained by the crew while the Shuttle was docked and during post-separation fly-around provided high-resolution images. The use of the 400 mm lens on the 35 mm camera was instrumental in obtaining the high-resolution imagery. STS-81 was the first Shuttle/Mir mission to use the 400 mm lens. Close-up still camera images acquired during docking and backaway were the best yet obtained of the docking mechanisms and provided for detailed analyses not previously possible.

Survey video taken with the Shuttle PLB cameras during crew sleep periods augmented the still photography, providing additional coverage and viewing directions. The PLB video imagery provided data used in the Kurs antenna position analysis. However, PLB Camera A had a substance on the center of the lens which resulted in glare effects, and PLB Camera B (Intensified TV Camera) did not provide high quality video for DTO-1118 applications. Critical procedural issues impacted the video acquisition for analysis of solar array motion for MiSDE. Required timing was not recorded on the PLB video for correlation with thruster firings. Also, the PLB video camera set-up (pan, tilt, zoom) was scheduled for a night pass and as a result, video of the Base Block array motion occurred after the Shuttle thruster firings scheduled to excite array motion.

Appendices C and D provide the film and video scenelists for the STS-81 mission. Appendix E lists the imagery sources for the images included in this Mission Report. Appendix F provides a diagram depicting the layout of film and photographic equipment specific to the STS-81 Mir survey.

2. MIR CONFIGURATION

This section provides an overall view of the Mir Station and identifies specific features that will be addressed in the following sections. In addition, a detailed assessment of the STS-81 configuration is presented, which involved identifying and labeling features directly from the photography. Features not previously identified, as well as changes to the known configuration, are identified on the following images. Due to good lighting conditions and the use of the 400 mm lens, the fly-around photography provided excellent coverage of Mir surfaces not seen during the docked phase.

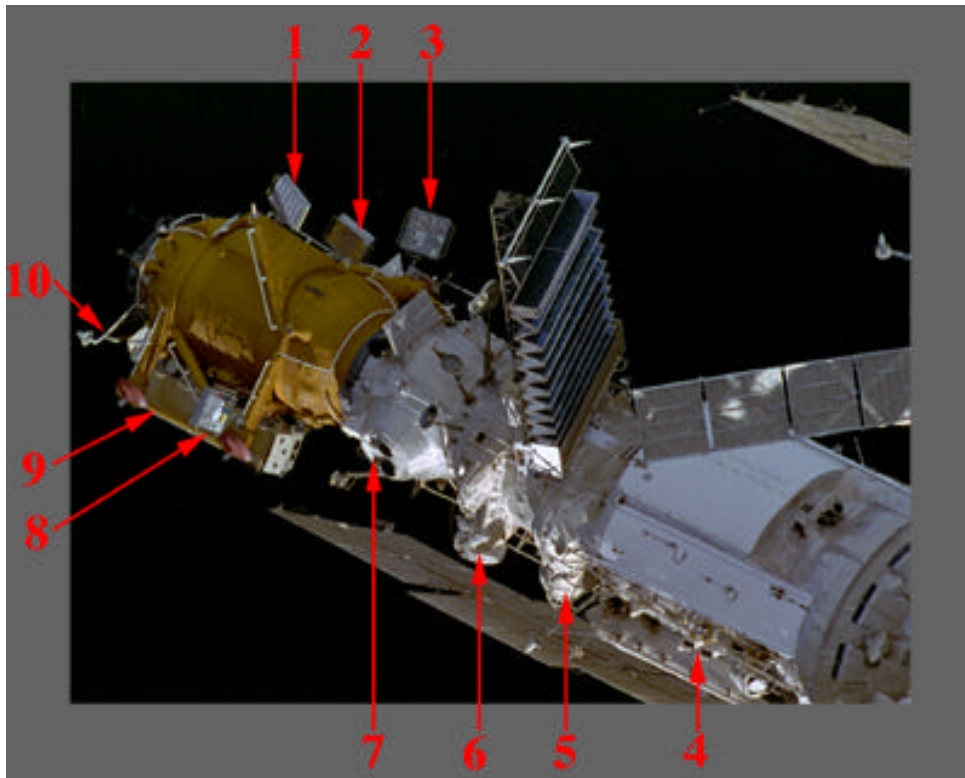


Figure 2.1 Docking Module / Kristall

- 1. Orbital Debris Collector (ODC) Experiment**
- 2. Polished Plate Micrometeoroid & Debris (PPMD) Experiment**
- 3. Passive Optical Sample Assembly II (POSA II)**
- 4. Solar Sensor**
- 5. "Rodnik" Water Tanks**
- 6. Unknown**
- 7. Photo Compartment**
- 8. Passive Optical Sample Assembly (POSA)**
- 9. Reusable Solar Array (RSA)**
- 10. Kurs Antenna***

*New feature identified during this mission.

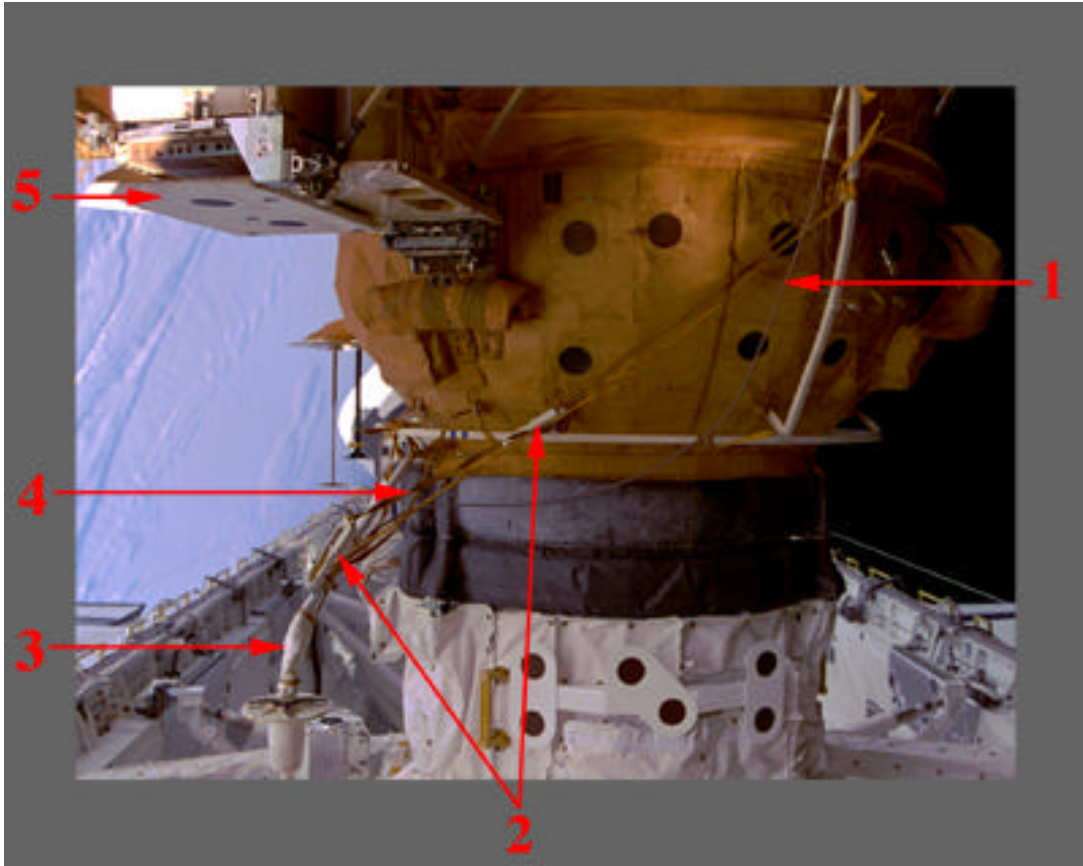


Figure 2.2 Docking Module / Orbiter Docking System (ODS)

- 1. Kurs Antenna***
- 2. Cable attached to Kurs Antenna***
- 3. Tethers used to hold Kurs Antenna in place***
- 4. Reusable Solar Array (RSA)**

*New feature identified during this mission.

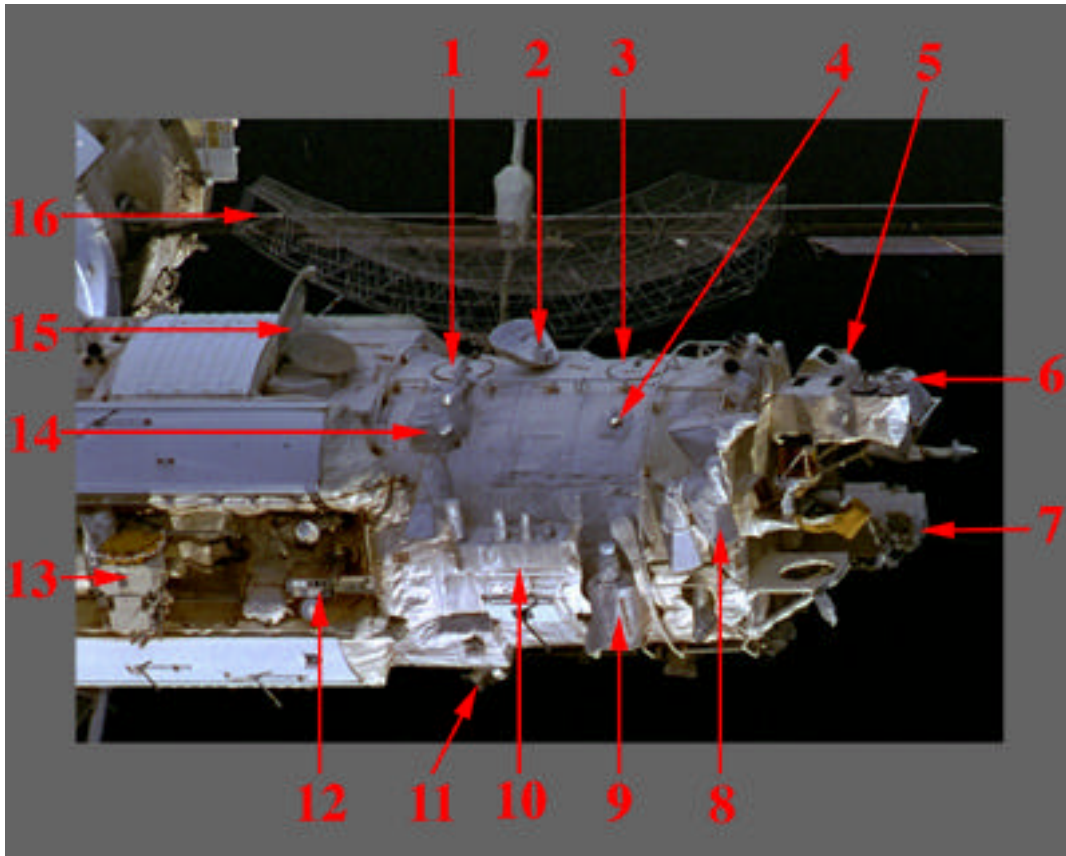


Figure 2.3 Priroda

1. LIDAR “Alissa” (Interior)
2. Radiometer R-400
3. “Survey” (Interior)
4. Antenna of Scientific Information Transfer Systems*
5. MSU-E Multi-channel Scanning Device*
6. MSU-SK Multi-channel Scanning Device*
7. Unknown*
8. IKAR-P Radiometer*
9. “Ozone-M” Equipment*
10. IKAR-N*
11. DK-33 Photometer*
12. Unknown*
13. Universal Mounting Platform*
14. Radiometer*
15. Delta-2P Radiometer
16. “Travers” Antenna

*New features identified during this mission.

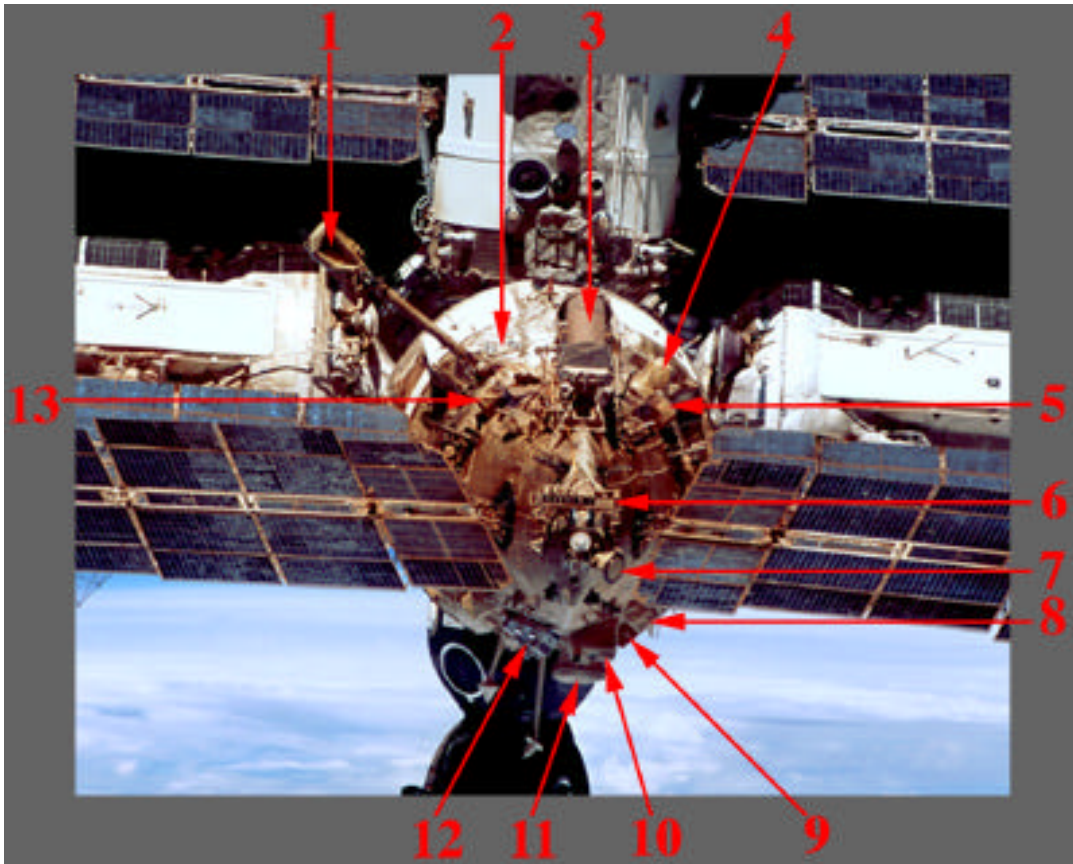


Figure 2.4 Spektr

1. "Astra" System Scanner
2. Unknown
3. "Miras" Solar Telescope and Spectrometer
4. Unknown
5. "Ryabina-4P" Hardware Detector Unit
6. Unknown
7. Unknown
8. "Ryabina-4P" Hardware Detector Unit
9. "Komza" Detector Unit
10. "Briz" Hardware
11. Installation Plate for Rotating Platform
12. European Science Exposure Facility (ESEF)
13. "Ryabina-4P" Hardware Detector Unit

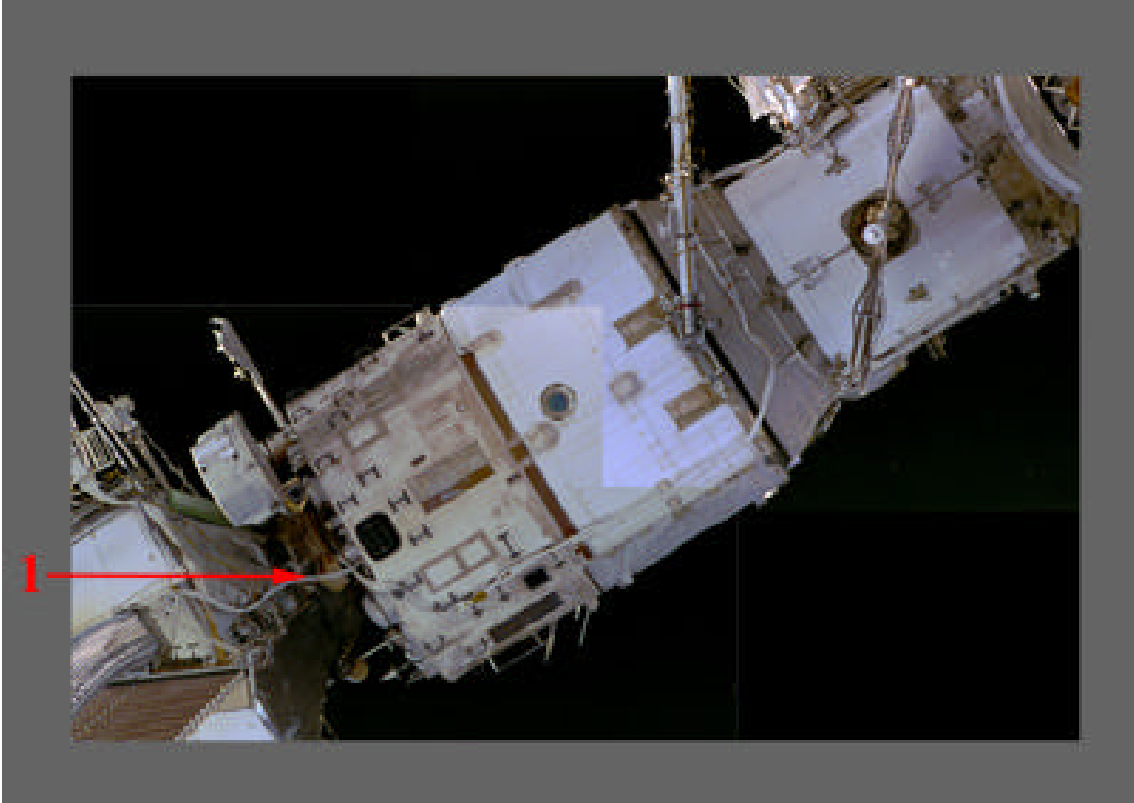


Figure 2.5 Base Block

Figure 2.5 is a mosaic of two photographs which have been combined to show the power cable [1] which appears to originate from the attach point of the Base Block SP#3 (in the upper right-hand corner of the frame) and extends to the attach point of the CSA on Kvant (in the lower left-hand corner of the frame).

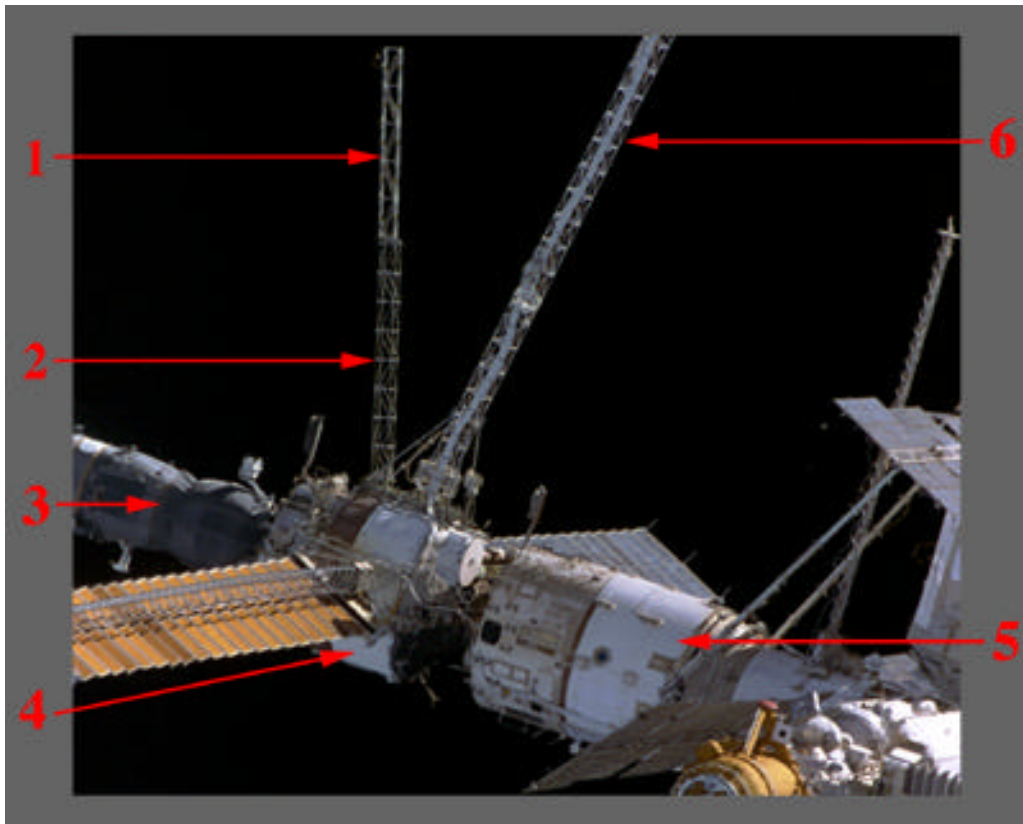


Figure 2.6 Kvant

- 1. “Rapana” Truss***
- 2. “Ferma-3” Truss**
- 3. Progress**
- 4. Kvant**
- 5. Base Block**
- 6. “Sofora” Truss**

*The location of the “Rapana” Truss has changed since the STS-79 mission. The “Rapana” Truss was formerly mounted at the location where the “Ferma-3” Truss is currently located. The “Rapana” truss was also temporarily stowed on the “Sofora” Truss while the “Ferma-3” Truss was being installed.

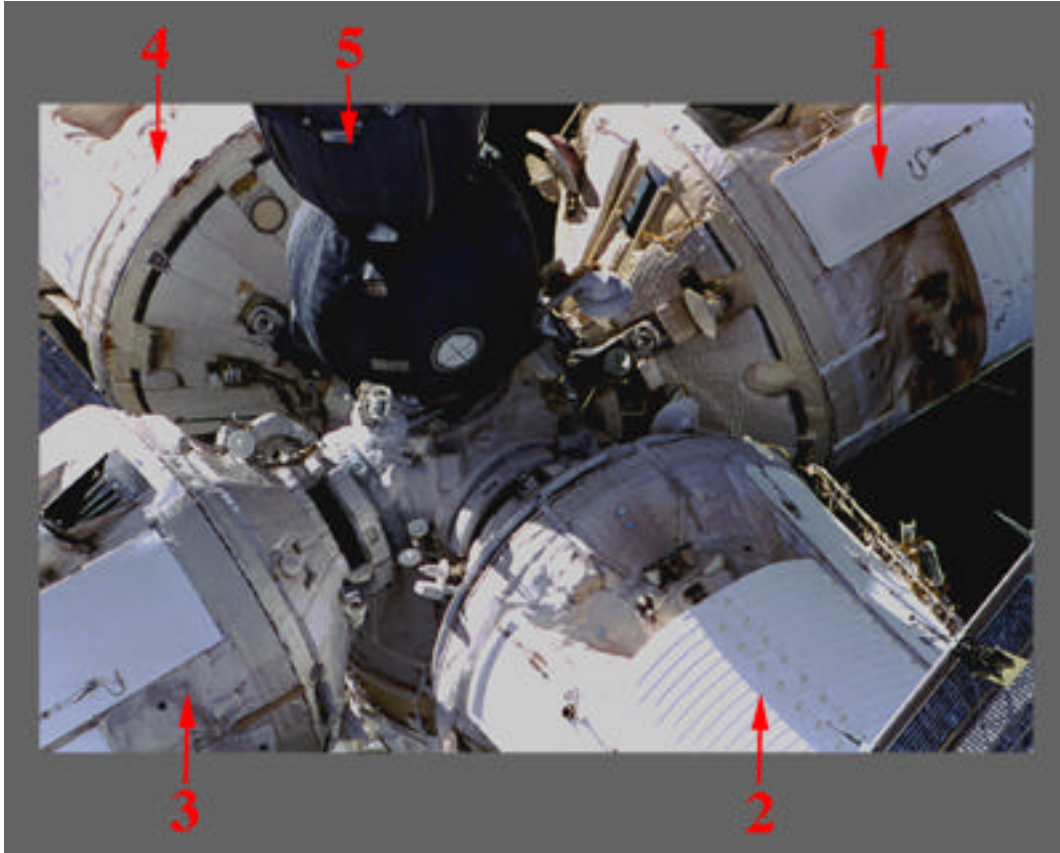


Figure 2.7 Docking Node

Figure 2.7 is a photograph of the multiport docking node where five of the six modules connect. The docking node is located at the end of the Base Block.

1. **Spektr**
2. **Kristall**
3. **Kvant-2**
4. **Priroda**
5. **Soyuz**

3. MIR SURFACE ASSESSMENT

The DTO-1118 survey of the visible Mir Station components was performed to identify areas of damage and discoloration. Structural anomalies, such as incomplete antenna deployment or retraction, are also identified. STS-81 imagery was compared to previous mission imagery to identify and characterize changes and validate earlier mission findings. In addition, much of the STS-81 imagery is of higher resolution than previous mission imagery, and reveals additional details of Mir surface conditions. Appendix B lists the visible damage and discoloration found in the STS-81 survey. The list serves as a cross-reference for damaged and discolored areas seen during STS-63, STS-71, STS-74, STS-76, and STS-79.

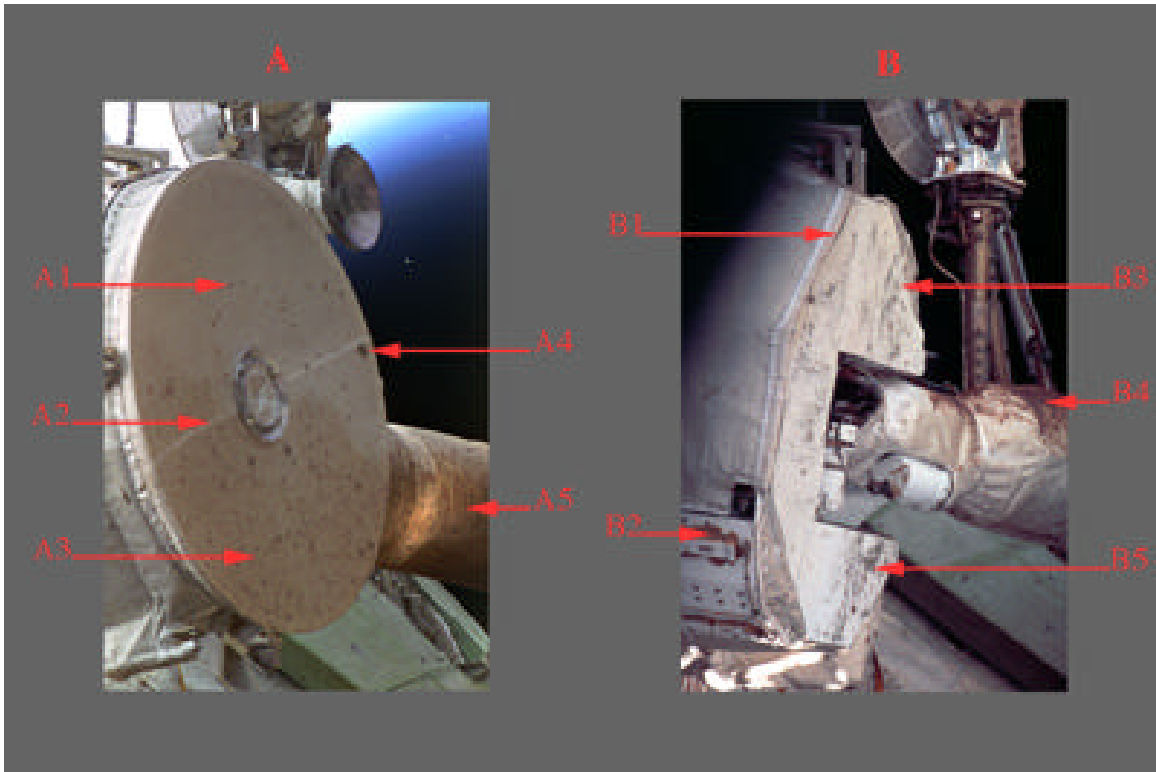


Figure 3.1a Mir Base Block - Luch antenna

The face side of the Luch antenna is shown in the A diagram. The back side of the Luch antenna is shown on the B diagram. The two sides have markedly different patterns of discoloration. The face side has a spotted pattern of discoloration [A3, A4, A5] with one preferential, circular pattern of dark spots [A1]. The back side has irregular discolorations [B2, B3, B4, B5]. A thermal blanket also has a detached edge [B1].

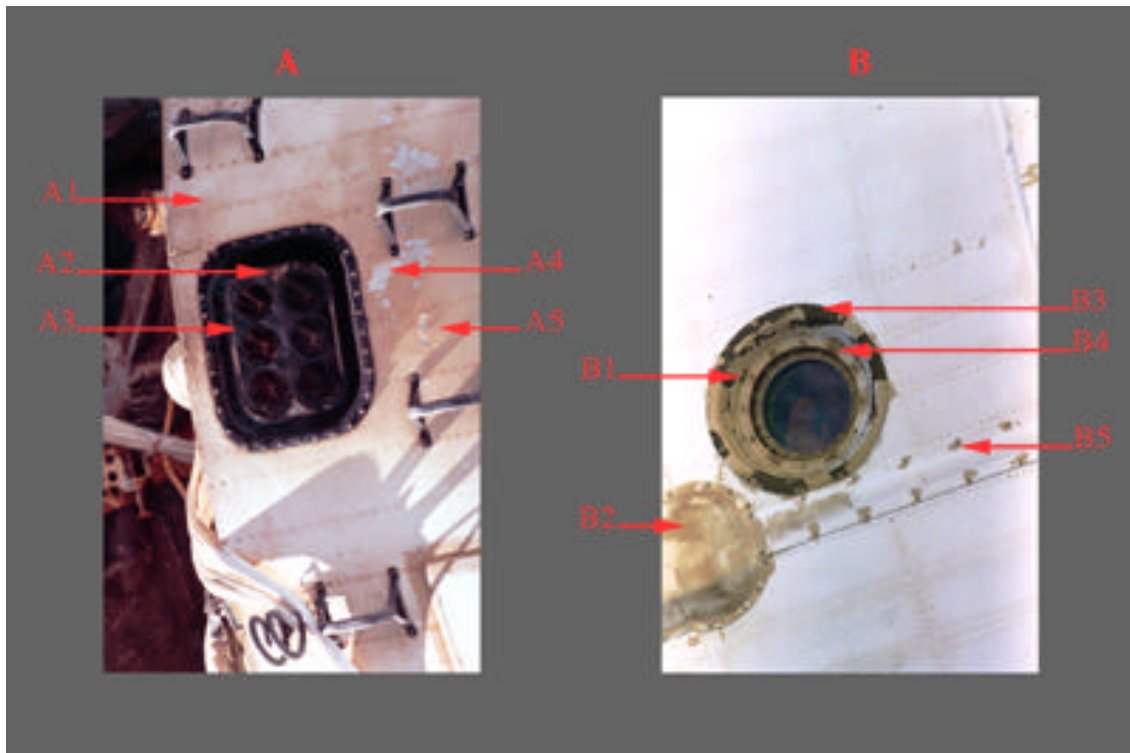


Figure 3.1b Mir Base Block - Thruster Engines and Optical Window

Thruster engines on the $-Z_B$ side of the Base Block are shown in the A diagram. The exterior window port on the $-Z_B$ side of the Base Block is shown in the B diagram. The surface effects are significantly different between these two areas on the same side of the Base Block.

The thruster engines and surrounding area are characterized by light orange discoloration [A1], discoloration on the metallic structure of the thruster engines [A2], blistering of the paint on the thruster engine structure [A3], and blistering and peeling of paint on the propulsion section [A4, A5]. The optical window and surrounding area are characterized by areas of peeling paint on the inner and outer metallic ring of the optical window [B1, B3], brown discoloration patches on the raised sections [B2] and around the support bolts of the window and module [B4, B5].

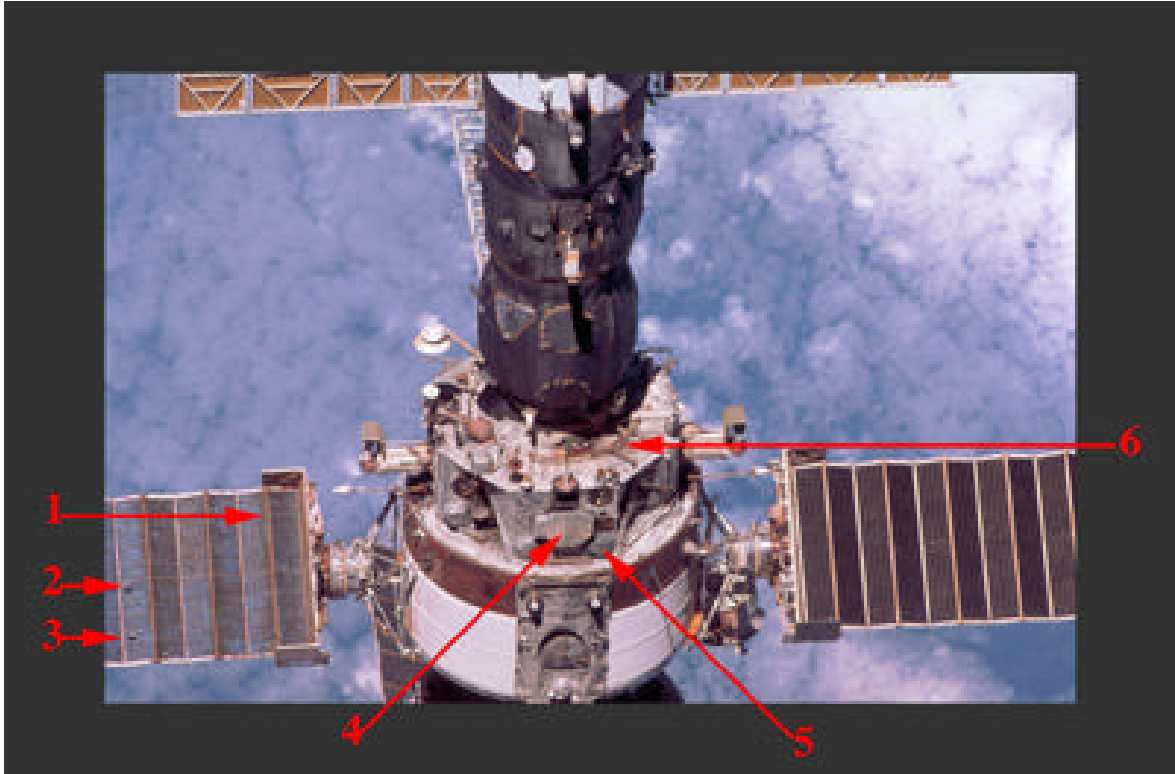
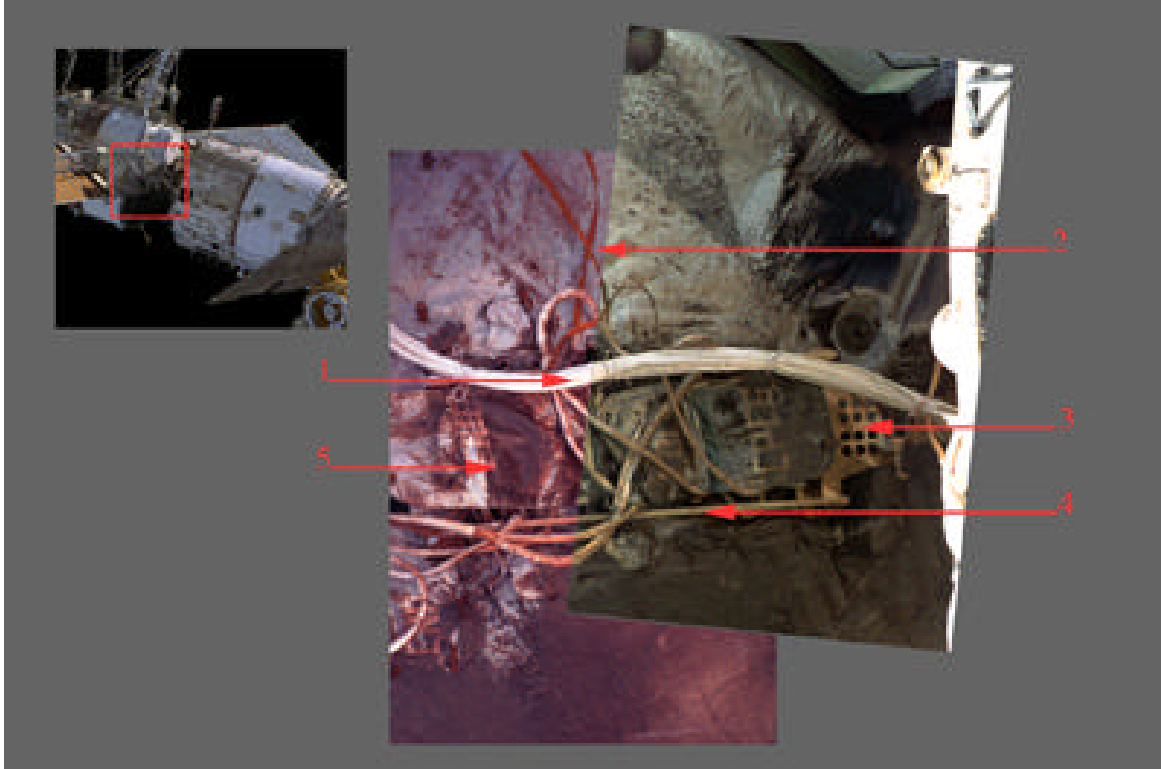


Figure 3.2a Kvant - Aft Facing Section of the Module in the $-Y_B$ Direction

The aft view of the Kvant module is shown in this image captured during the fly-around. The following surface features are identified:

- Dark brown discoloration around the support structure of the solar array. [1]
- Detachment of S/A cells. [2, 3]
- Discoloration and blistering on the thermal blanket. [4, 5, 6]



**Figure 3.2b Kvant - Docked Section Aft of the Base Block in the
-Z_B Direction**

The conical-shaped section of the Kvant module is shown as a mosaic of two 35 mm images. Various cables that connect the Kvant and Base Block modules are seen in this image. Discolorations observed in the image are a dark spot on the cable connecting the CSA and the Base Block [1], and dark color discoloration on the metallic structure [3], support structure [4] and the thermal blanket [5].

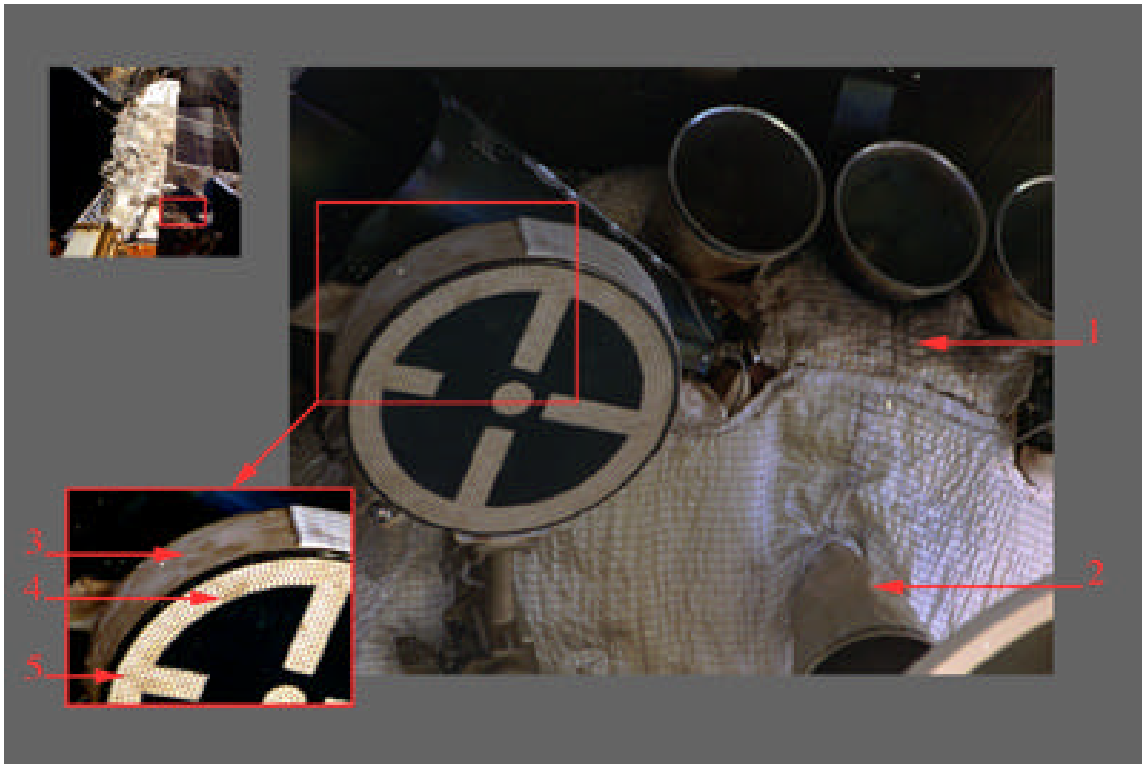


**Figure 3.3a Kristall - Buran TV Target and Thruster Engines in the
-X_B Direction**

In this detailed view, the Buran TV target and the mooring and stabilization engines in the -X_B direction of the Kristall module are seen. The following surface effects are identified:

- Discoloration and charring of the thermal blanket around the thruster engines. [1]
- Patches of discoloration and possible deposition on the edge and face sides of the target. [3, 4, 5]



**Figure 3.3b Kristall - Mooring and Stabilization Engines in the
-XB Direction**

Detailed views of the mooring and stabilization engines and the interior of the nozzles are shown. The image in the upper left corner is a reference image from STS-76. The following surface effects are identified from the STS-81 image:

- Discoloration or scratch marks on the outer edge of the thruster engine nozzles. [1]
- Discoloration or deposition on the interior wall of the thruster engine nozzles. [2, 3, 4]
- Faint and dark color patches and blistering of the thermal blanket. [5, 6]
- Peculiar color patterns on metallic surfaces. [7]



Figure 3.3c Kristall - Igla Antenna Cable Mechanism in the -XB Direction

This is a detailed view of an Igla antenna's cable mechanism on the Kristall module. In this view, the outer jacket of the cable shows a possible burn-through. The inset image is an enhanced illustration of this damage. The following surface effects are identified:

- Dark color discoloration or charred area on the cable. [1]
- A possible burn-through section of the cable. [2]
- A possible break in the cable harness. [3]

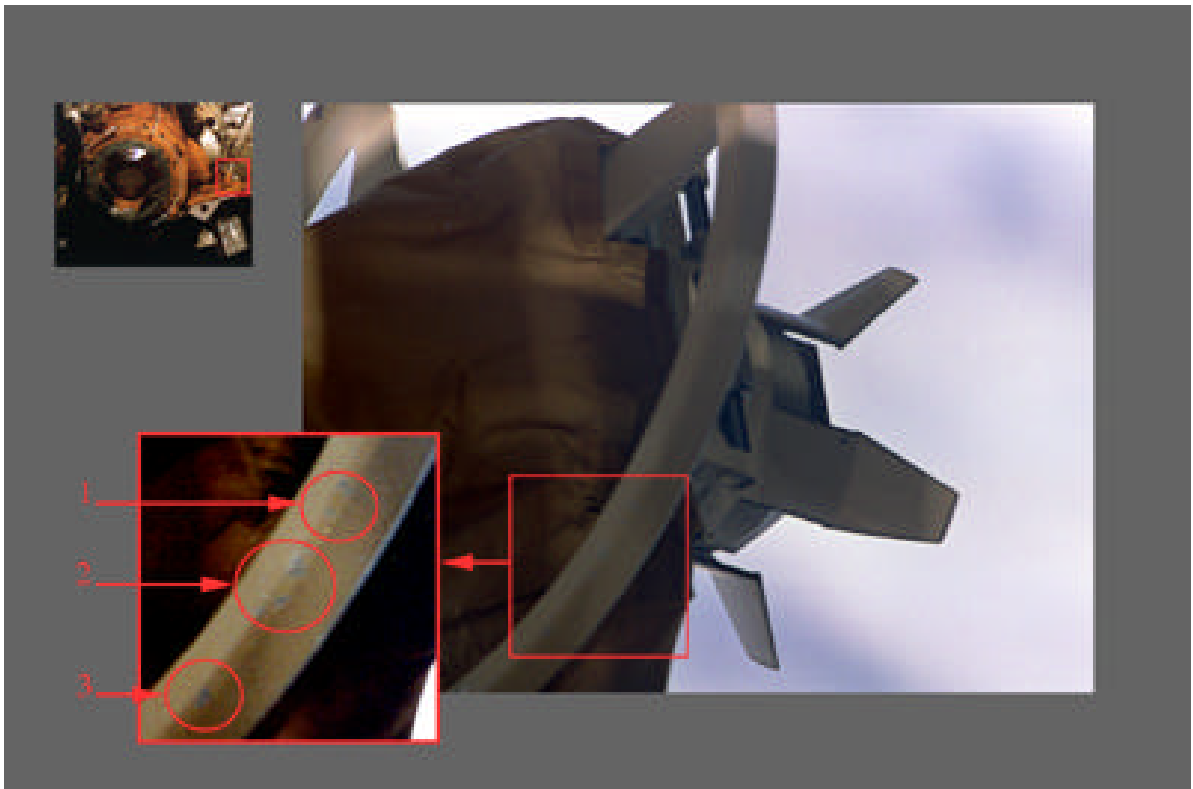


Figure 3.4a Docking Module - ROEU-PDA

This is a detailed view of the Remotely Operated Electrical Umbilical (ROEU) Payload Disconnect Assembly (PDA) located on the Docking Module. In this view, the handrail on the ROEU-PDA shows prominent scratch marks or dents as shown in items 1, 2, and 3.



Figure 3.4b Docking Module - HARR

This is a detailed view of the Hemispherical Array Retroreflector (HARR) #5 located on the Docking Module. In this view, the HARR and the support structure's backplate are seen. The metallic backplate shows a color pattern similar to that of an interference pattern of the reflected light. A similar color pattern is also seen on the SA attach plate on the Spektr module (See Figure 3.5a).

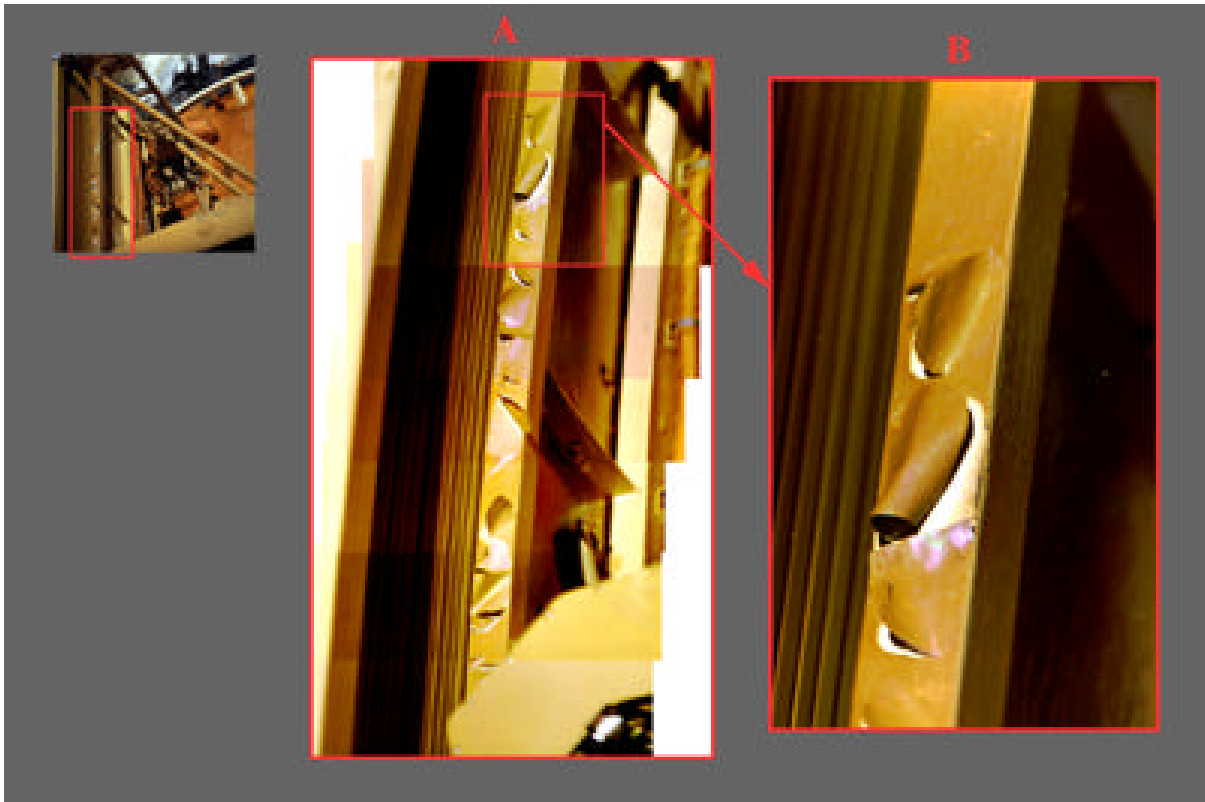


Figure 3.4c Docking Module - RSA

This is a detailed view of the Reusable Solar Array (RSA) carrier on the Docking Module. This view shows peeling paint on the RSA carrier's support structure. Image A is a mosaic of six individual 35 mm photographs obtained during this mission using a 400 mm lens. Image B is one individual photograph from this mosaic sequence. As seen in image B, this peeling paint has linear and smooth rounded edges. Also, most of the paint remains attached, with some pieces of peeled paint curved inward and other pieces curved outward.

A comparison of the paint peeling on STS-76 versus STS-81 is shown in Figure 3.4d.

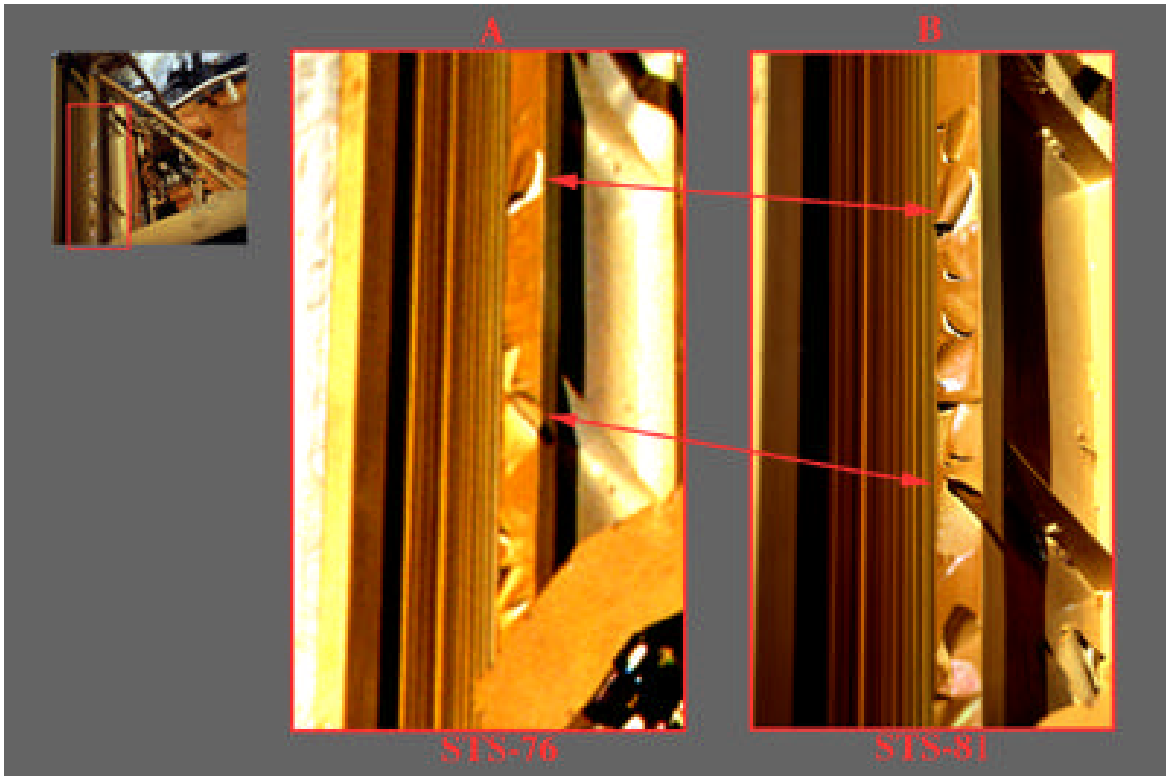


Figure 3.4d Docking Module - Comparison of RSA: STS-76 vs STS-81

Detailed views of the Reusable Solar Array (RSA) carrier from two different missions are shown in Figure 3.4d. The image obtained during the STS-76 mission is shown in the A diagram and the image obtained during the STS-81 mission is shown in the B diagram. It is apparent from these images that the amount of peeling paint on this upper part of the RSA carrier increased during the 10 months between these two missions. During STS-76 (image A), about 20% of the paint from the RSA carrier was found to be peeled. During STS-81 (image B), about 80% of the paint from the same RSA carrier edge appears to be peeled.

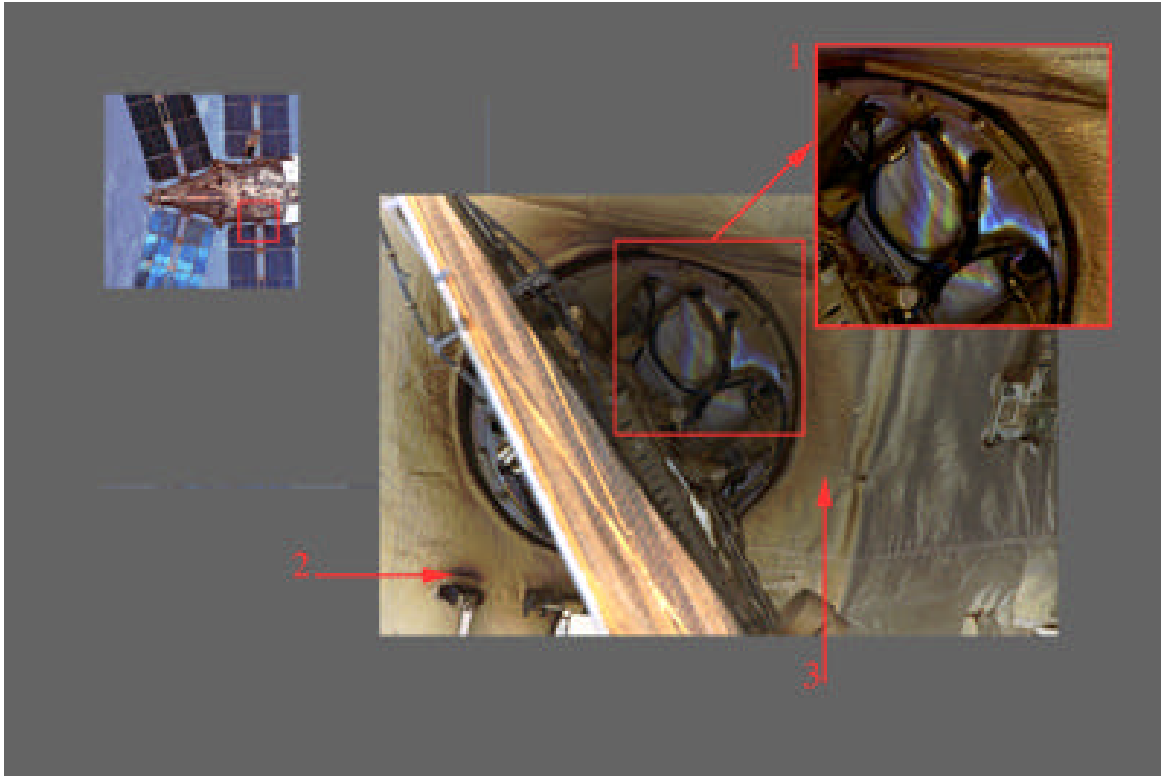


Figure 3.5a Spektr - Solar Array Attach Point: SP#2

This is detailed view of the solar array attach point on the Spektr module. In this view, the attach point of the SP#2 of the Spektr module is shown [1]. The attach area has a color pattern similar to interference of reflected light. A similar color pattern was also identified on a backplate located on the Docking Module (see Figure 3.4b). Discoloration of the thermal blanket are also shown [2, 3].

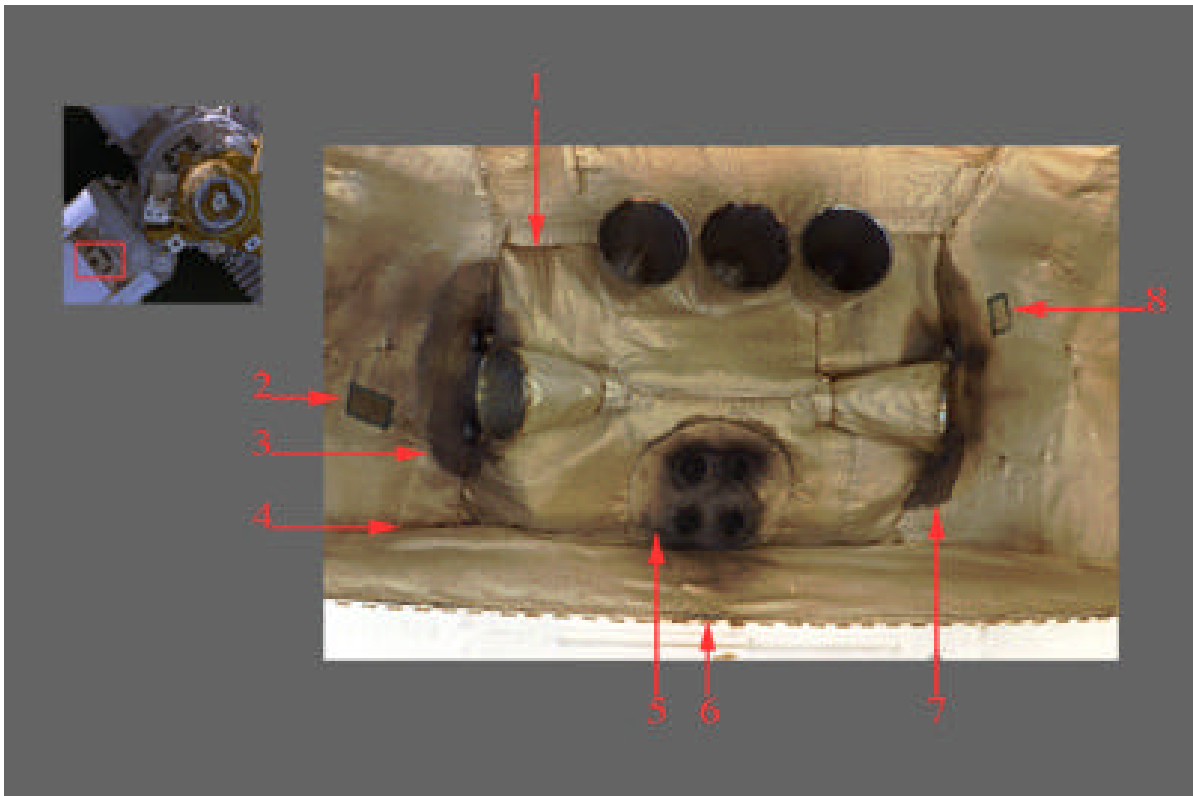


Figure 3.5b Spektr - Thruster Engines

This is a detailed image of the thruster engines on the Spektr module. In this image, the thruster engines located aft of the Spektr module in the $-Z_B$ direction are shown. The following surface effects are identified:

- Dark discolorations of the thermal blanket and the areas beneath the engine cone. [1, 3, 4, 7]
- Attachments / patches on the thermal blanket. [2, 8]
- Charred areas of the thermal blanket in the vicinity of the engine exhaust. [5]
- The thermal blanket has small areas which appears to be detached from the surface. [6]

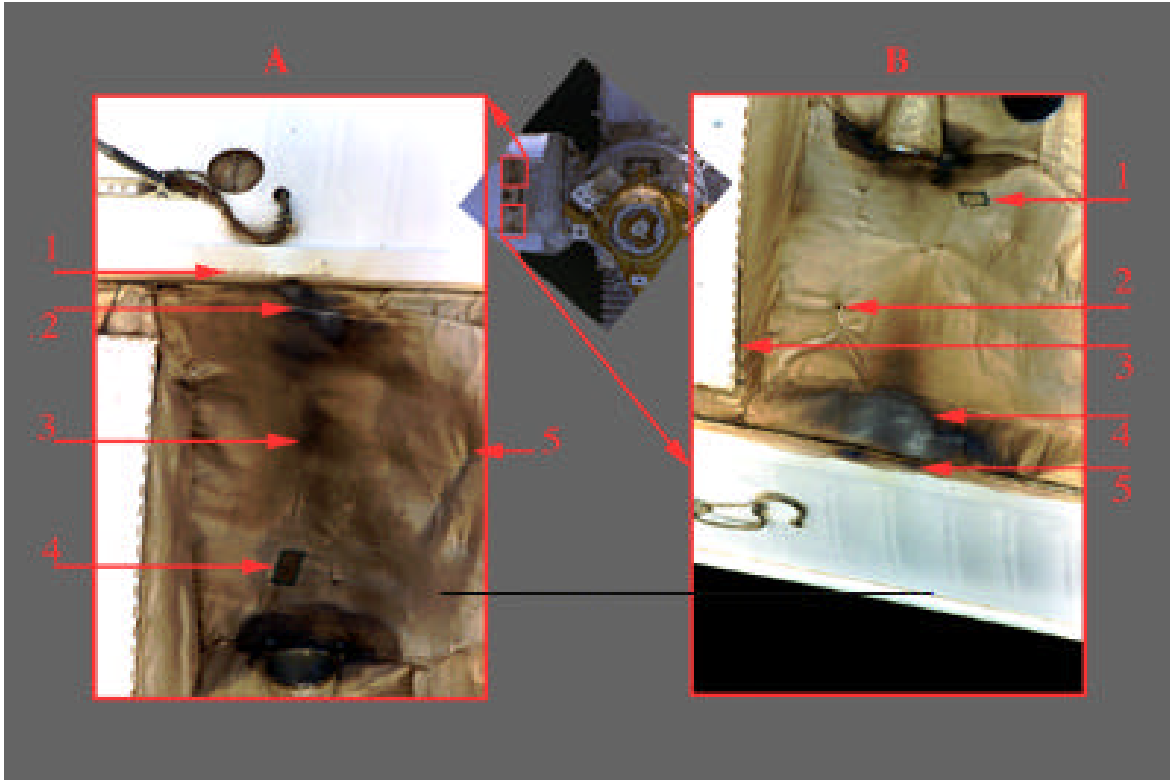


Figure 3.5c Spektr - Thruster Engines and Thermal Blankets

These images show the effects of the thruster plumes from the engines onto the thermal blanket. Two images are shown in this figure. Image A is the view of the thermal blanket in the $+Z_B$ direction. Image B is the view of the thermal blanket in the $-Z_B$ direction. The following surface effects are identified:

- Discoloration on the metallic surface in the plume line-of-sight. [A1]
- Dark discolorations / charred effects on the thermal blanket. [A2, A3, B4]
- Detailed views of attachments / patches. [A4, B1]
- Possible holes in the thermal blanket. [A5, B2]
- A radiator panel that appears to be detached at the edge. [B3]
- Charred effect on the metallic surface in the plume line-of-sight. [B5]

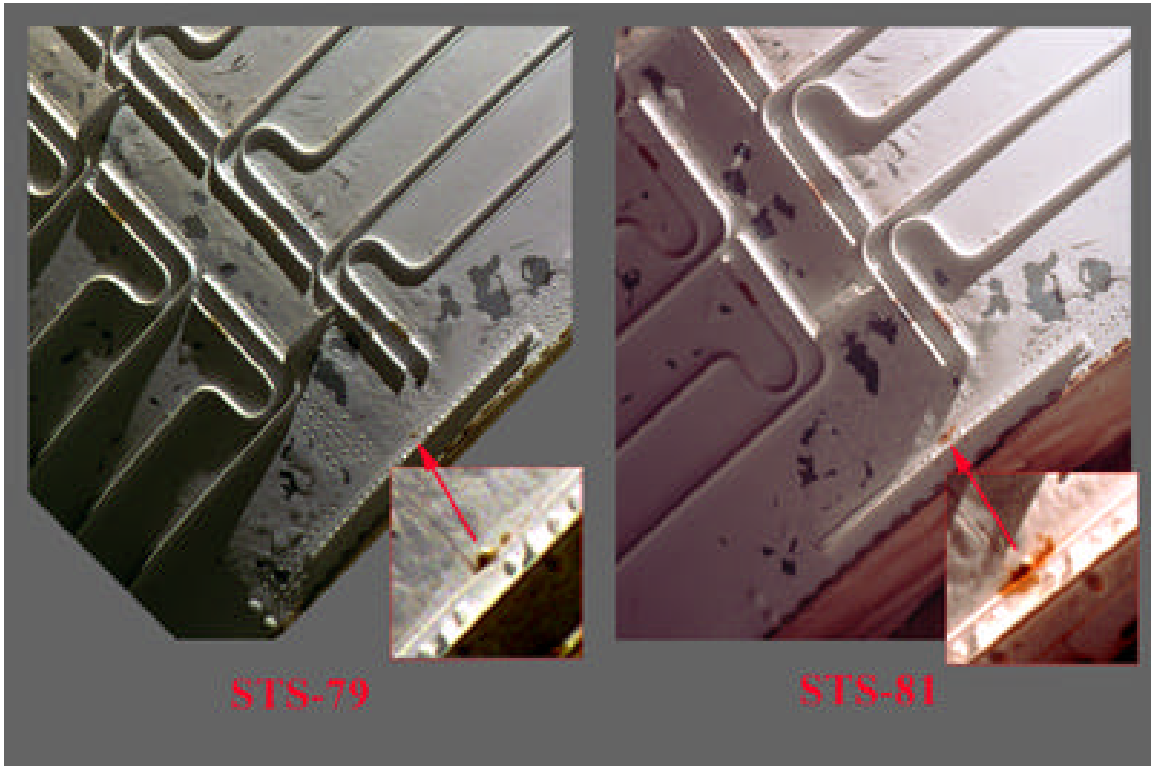


Figure 3.5d Spektr - Comparison of a Possible Radiator Leak: STS-79 vs STS-81

In this figure, two different Spektr radiator images that were obtained four months apart on STS-79 (left) and STS-81 (right) are shown. The progression of the small leak in the radiator is shown in the enlarged inserts to the STS-79 and STS-81 imagery. The small leak in the Spektr radiator was first identified in the STS-81 high resolution imagery, obtained with the 35 mm camera and 400 mm lens while the Shuttle was docked to Mir. This leak shows as an orange-appearing color in the imagery. The leak appears to originate at a rivet which is in the corner of a radiator panel and adjacent to a structural reinforcement. A review of imagery showed the leak existed at the time of STS-76 and STS-79, but the affected area was very small at those times and went undetected in the imagery reviews. On STS-74, the imagery showed no apparent discoloration. By STS-76, the discolored area was isolated to the rivet only. On STS-79, the leak extended to include a small area along the edge of the structural reinforcement, and by STS-81 the affected area extended across the edge, and along the edge in both directions from the rivet. The size of the affected area was determined from the STS-81 imagery to be approximately 7 sq. cm.

Note also the regions of additional paint peeling on the radiator between STS-79 and STS-81. The STS-79 Mission Report identified both missing and blistered paint on the radiator.

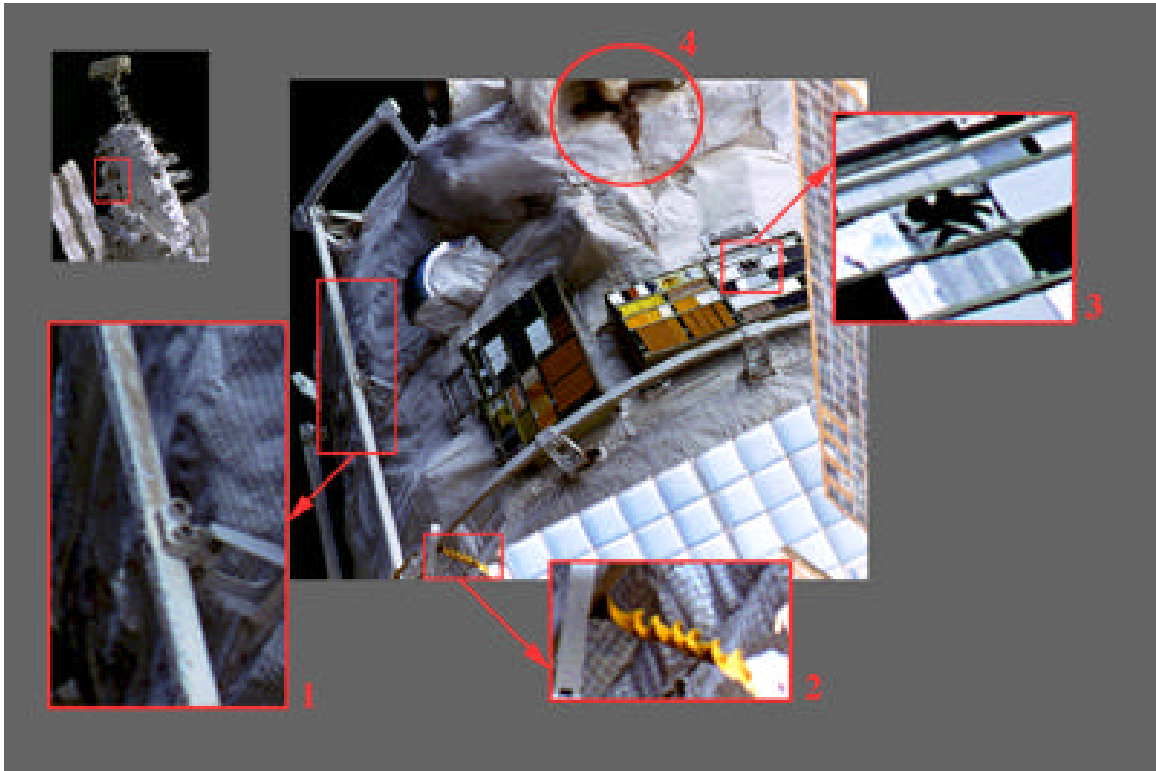


Figure 3.6 Kvant-2 - MSRE

In this figure, the forward section of the Kvant-2 module is shown. The “Komplast” cassettes mounted on the -ZB side of the Kvant-2 module are clearly visible. The Mir Sample Return Experiment (MSRE) is also seen. The inset images show the following:

- Dark discoloration on the EVA handrail. [1]
- A twisted cord that is attached to the MSRE, and a possible tear on MSRE. [2]
- One of the test blocks on the “Komplast” appears to be broken. [3]
- Dark discoloration on the seams / folds of the thermal blanket. [4]

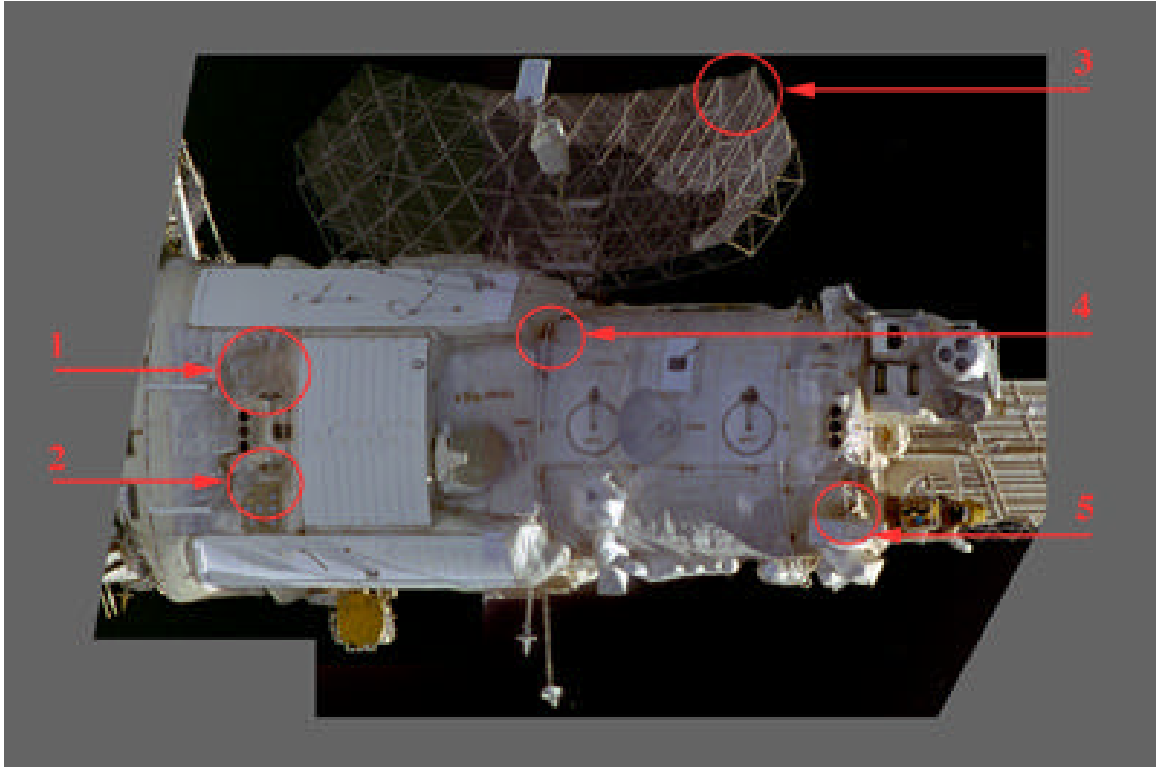


Figure 3.7 Priroda as seen from the -XB Direction

This figure is a mosaic of two photographs of the Priroda module as seen from the -XB direction. The following surface effects and features are identified:

- Discoloration on the thermal blanket near the aft thruster engines. [1, 2]
- Three of the trusses of the SAR antenna have bends. [3]
- Dark discoloration on the thermal blanket near the EVA attach point [4] and beneath the EVA handrail [5].

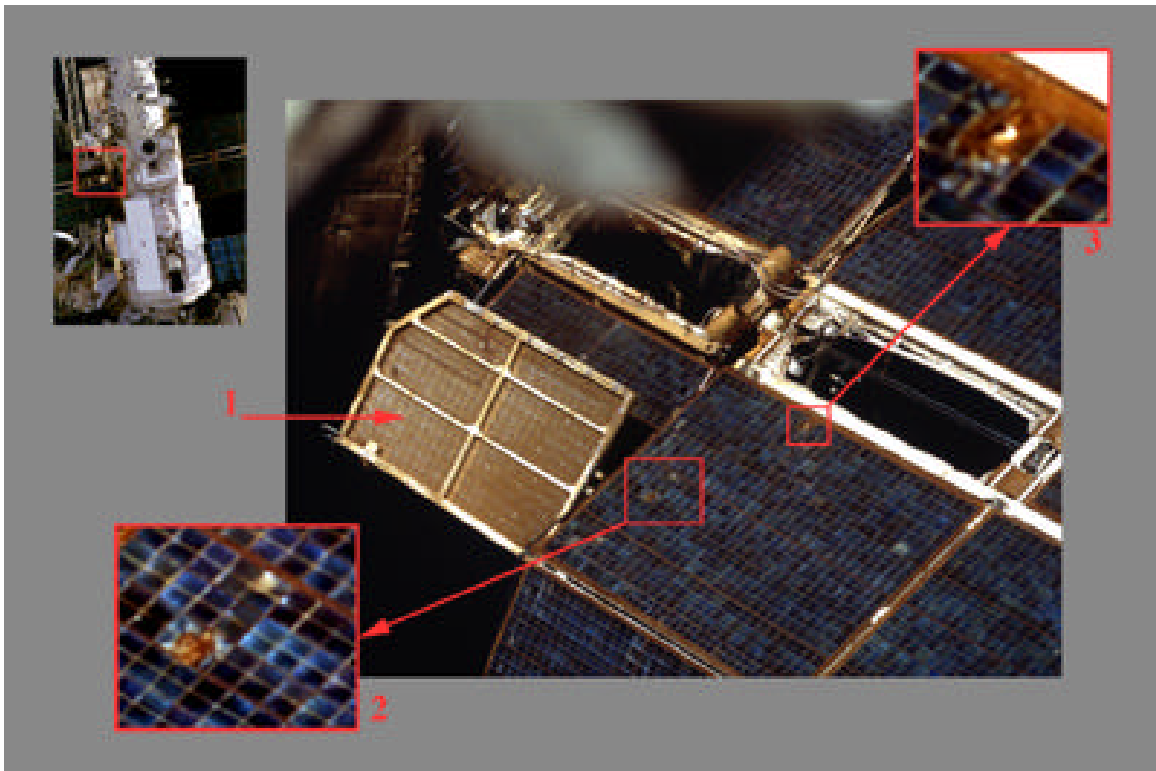


Figure 3.8a Kvant-2 - Solar Array: SP#2

This figure is a detailed view of the Kvant-2's SP#2 solar array. From this view and orientation of the array, two new features for this array are identified. The inset images show the splattered appearance of the cells. Six to eight adjacent cells appear to be affected for each of the two features. The inset on the right indicates the presence of a hole, which suggests penetration of some impact material.

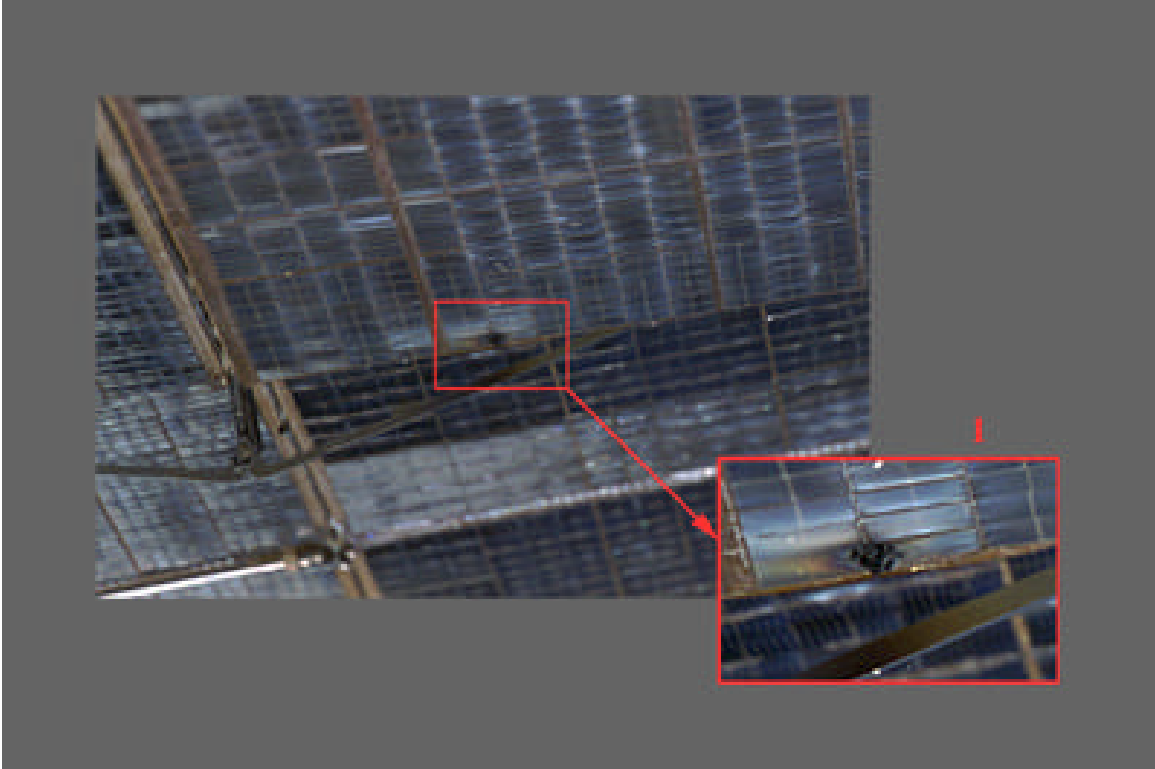


Figure 3.8b Base Block - Solar Array

This figure provides a detailed view of the underside of the solar array panel. The image insert provides an enhanced image showing apparent damage to the metallic support structure. The source cause of this damage is not known.

4. DOCKING MECHANISM ASSESSMENT

Imagery surveys of the docking mechanism were performed to verify its condition. In addition, a target viewing assessment was conducted to evaluate the performance of video cameras used during the approach. Analyses of these views help evaluate camera usage for ISS proximity operations. For the first time since STS-74 (November 1995), close-up still photography was taken of the Mir docking mechanism during approach and during backaway. These close-up images provided the highest resolution imagery of the docking mechanism to date.

During STS-81 approach, photography of the docking mechanism was taken with the Nikon 35 mm camera and the 400 mm lens. An image, taken at a distance of approximately 215 feet, is shown as Figure 4.1. The image is a face-on view of the docking mechanism and shows the docking mechanism to be in good condition, with latches in proper position.



Figure 4.1 Photo of Docking Mechanism during Approach

The only identifiable discoloration is on the non-axial docking target backplate as shown in Figure 4.1 and Figure 4.2. The discoloration, also observed on STS-79 imagery, is detectable since the stand-off target apparently shielded the backplate and, as a result, there is a narrow strip that is less discolored. A second strip of less discoloration also exists, indicating there may have been two sources of discoloration, or the same source from two separate orientations.



Figure 4.2 Enhanced Image Showing Discoloration and Shielded Strip on Non-Axial Target Backplate

Although the docking ring and the target are clearly visible, the video imagery is not of sufficient quality (due to poor lighting) to perform an assessment of the docking mechanism during the docking phase. However, the close-up images taken with the 35 mm film camera during approach show the structural latches, capture latches, alignment guides, laser retroreflectors, electrical socket plugs, and the centerline target backplate and stand-off target cross to be in excellent condition. A composite image of the full docking ring has been formed from two separate images and is shown as Figure 4.3.

Centerline video camera imagery taken during docking also shows the centerline docking target to be in good condition and no discoloration of the target is indicated. However the docking target, the stand-off target, the target alignment guide, and the centerline camera axis do not appear to be in perfect alignment. The analysis of this misalignment is described in Section 8 of this report.

Several close-up images were taken during backaway with the 35 mm camera from the Shuttle overhead windows. One of the highest resolution images of the docking mechanism is shown in Figure 4.4. Figure 4.4 is the portion covering the docking ring in the original image and has been enhanced in brightness and contrast from the digitized image. Figure 4.4 and similar images show the structural latches, capture latches, alignment guides, centerline target, laser retroreflectors, and electrical connectors in considerable detail. Each part of the docking mechanism appears to be in excellent condition for the subsequent Shuttle docking to Mir. The highest resolution images show possible traces of discoloration on the docking ring adjacent to some of the structural latches. There are also small, isolated traces of apparent discoloration in other locations. The traces of apparent discoloration observed on the docking ring do not extend to the electrical connectors.

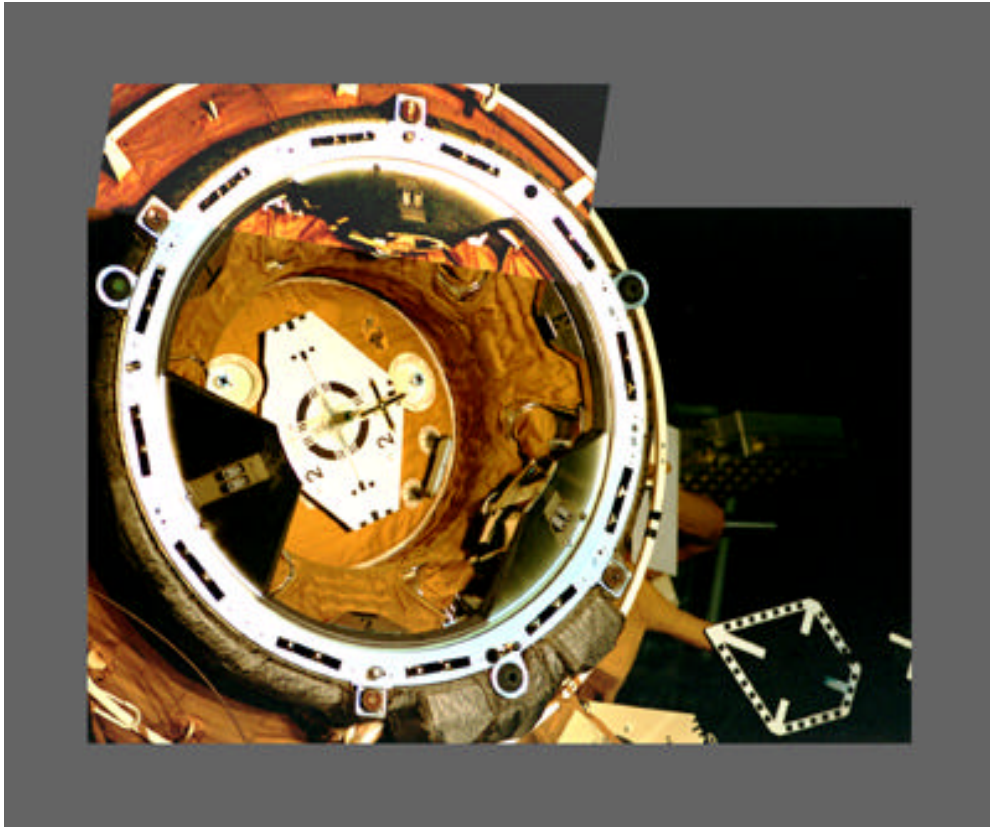


Figure 4.3 Composite Image of Docking Mechanism during Approach

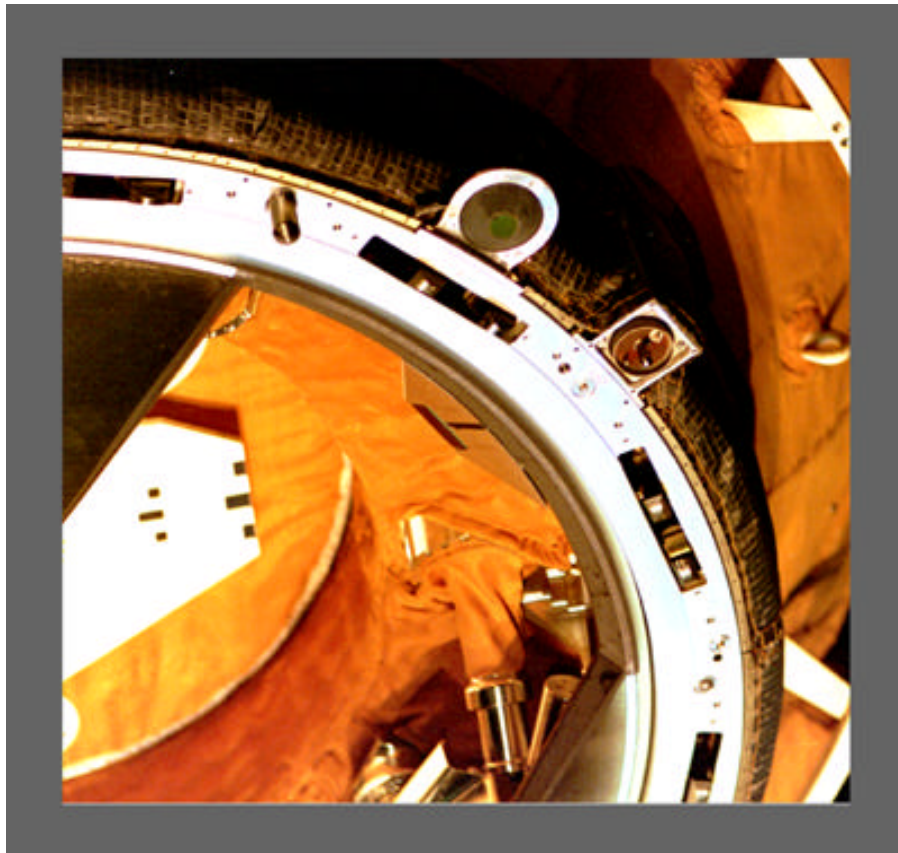


Figure 4.4 Image of Portion of Docking Mechanism during Backaway

5. MIR STRUCTURAL DYNAMICS EXPERIMENT SOLAR ARRAY MOTION

Image analyses of the motion of Mir solar arrays have been performed since the first Shuttle docking flight to Mir, STS-71. Frequency and amplitude measurements from imagery have been made for the Kvant SP#1, Kvant-2 SP#2, Base Block SP#2, Spektr SP#2, and the Cooperative Solar Array (CSA). During STS-71 and STS-74, tests were conducted with the firing of Shuttle Reaction Control System (RCS) thrusters during the time the Shuttle was docked and the amplitude and frequency of solar array motion was determined. Measurements have been correlated to the times of Shuttle thruster firings through the use of timing on the video. These data on solar array motion were provided to the JSC Structures and Mechanics Division for use in structural dynamics modal analyses and support to International Space Station (ISS) loads verification.

The Mir Structural Dynamics Experiment (MiSDE) is a risk mitigation experiment for the ISS. The purpose of the experiment is to obtain dynamic, structural response data on the Mir for validation of ISS loads and dynamics models. Accelerometers are placed throughout the Mir and measure accelerations in three dimensions as the Mir responds to a variety of dynamic load stimuli. Crew exercise activities on-board the Mir and timed thruster firings from the Shuttle and Mir are the most notable sources of perturbation. In addition to the accelerometers, video of solar array motion is captured during the timed thruster firings for correlation with the accelerometer response.

5.1 Solar Array Video Data Acquisition

Acquisition procedures were developed to obtain data and perform analyses of the motion of Kvant-2 SP#2 during a single thruster firing sequence from the Mir and the motion of Base Block SP#2 during five controlled thruster firing sequences from the Shuttle.

Two simultaneous video camera sequences were acquired to obtain a three-dimensional solution of the motion of a point on the array. Video at both the array tip and the attach point at the module allows the removal of module motion from the motion of the array. During the Shuttle thruster firings, PLB Cameras A and D record motion at the tip of Base Block SP#2, while Cameras B and C record motion at the array attach point. The video of camera pairs A/D and B/C were muxed. During Mir thruster firings, the same camera set-up was used to record the motion of the Kvant-2 SP#2.

Once each camera acquired the array, camera pan and tilt settings were fixed for the duration of the thruster firing sequence. At the conclusion of the sequence, the camera views were demultiplexed. Each camera's pan and tilt was then adjusted to acquire video of the Docking Module. The zoom of the camera was held constant during this procedure so that features of known size on the Docking Module could be used to establish the camera scale parameter in the data analysis.

Data acquisition was to be carried out for five Shuttle firing sequences and one Mir thruster firing sequence. However, several problems were experienced in the acquisition of the required video data of the solar arrays:

- a. The allocated time for the crew to perform the set-up of the cameras occurred during night passes and the crew could not see sufficient detail in the video image to align the cameras and optimize the solar arrays in the camera field-of-view. In the case of Base Block SP#2, the camera set-up could not be completed until the beginning of the daylight pass. Unfortunately, the first two Shuttle thruster firing

-
- sequences had already occurred. Video was obtained of the last three sequences. The motion from two of these three sequences is barely perceptible in the video.
- b. To correlate solar array motion with thruster firings and accelerometer data, and to correlate tip and attach point motions, it is necessary to have IRIG timing recorded onto the tapes which contain the MiSDE video. However, synchronous timing was not obtained.
 - c. A smudge was present on the center of the lens of camera A. This smudge caused a permanent glare, and reductions in contrast in the smudged region were present in all MiSDE video utilizing camera A.

As a result of the noted problems, the Mir thruster firing video was the first video selected for analysis. Thirty seconds of video was selected for analysis of the array motion. This sequence of video was selected to encompass a span of time prior to, during, and after the Mir thruster firing sequence. A muxed video frame used in the analysis of the Kvant-2 SP#2 motion is shown in Figure 5.1, with the tracked point labeled as 'A'. This frame is a muxed view of video images from cameras A and D.

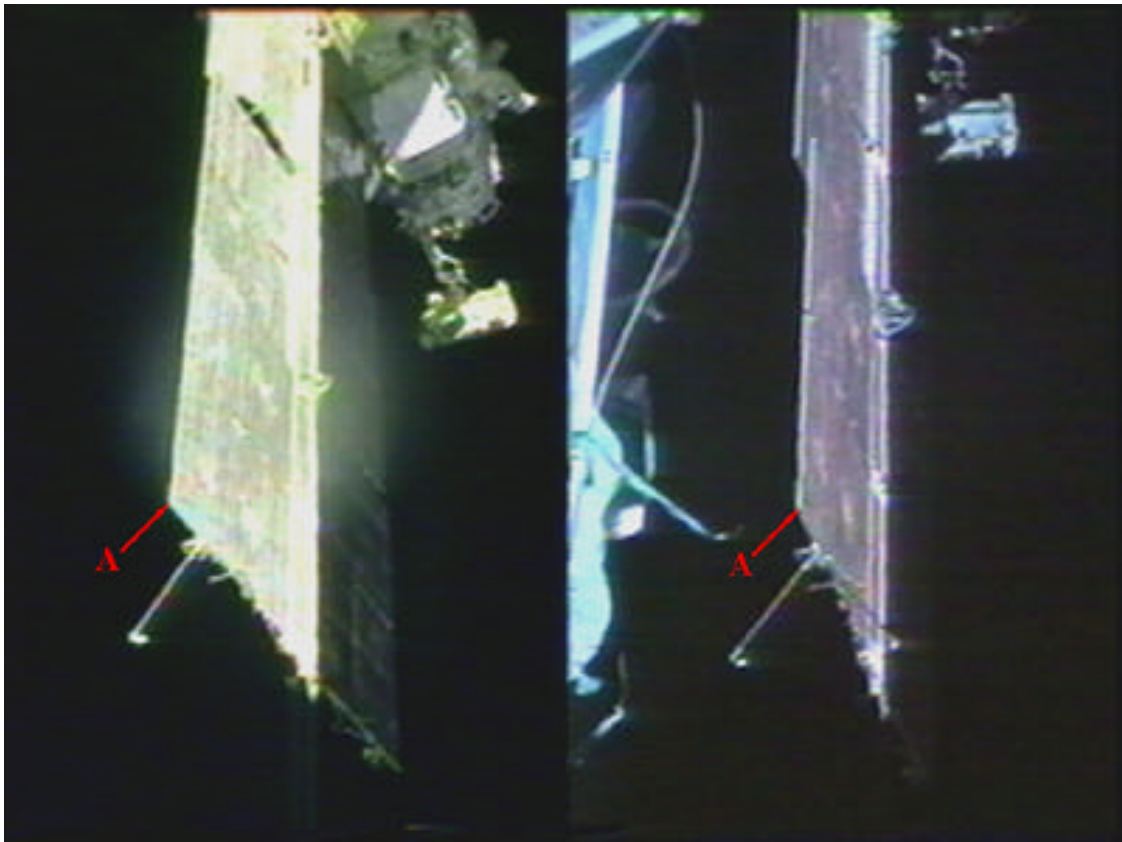


Figure 5.1 A Muxed Video Frame Used in Motion Analysis of Kvant-2 SP#2

5.2 Data Analysis Approach

To extract data from the recorded video of Kvant-2 SP#2, 3 methods were attempted: line tracking, point tracking, and manual image data extraction.

The line tracking software allows the user to define the end points of lines to be tracked. The program then uses a Canny edge detection filter to improve the “fit” of the line to be tracked. This program works best in high contrast situations and has been highly successful in previous solar array motion analyses. The intersections of lines determine the points of interest on each frame. For the STS-81 video, however, the lines of the array edges could not be tracked with accuracy due to insufficient video quality. The video quality issue is manifested as frequent and random shifts in the image pixel coordinates of the array. Figure 5.2 shows an example of this video quality deficiency in the region containing the point of interest. Due to the pixel shifts, the line tracking algorithm could not reliably determine an edge to track.

The point tracking software, allows the user to select a point to be tracked, a region of interest containing that point (to reduce computation time compared to a full frame of video), and a computational area of user-defined size. This computational area is compared to areas of the same size in the region of interest using a normalized cross-correlation function. The center of the area with the highest correlation represents the point being tracked. The X and Y position data, as well as a measure of the correlation between each of the frames, are saved to a data file. The poor quality of the video also hampered the point tracking algorithm. As the point tracking software compares video frames to determine the location of the point of interest, image quality changes of the nature shown in Figure 5.2 made reliable correlation from frame to frame impossible. The lack of reliable correlation results in a loss of tracking. Several methods were undertaken in an attempt to overcome this problem. Image enhancement, preferential edge detection, and an edge detection/image difference filter was utilized. None of the enhancements provided sufficient improvement to the data to allow reliable tracking of the array tip.

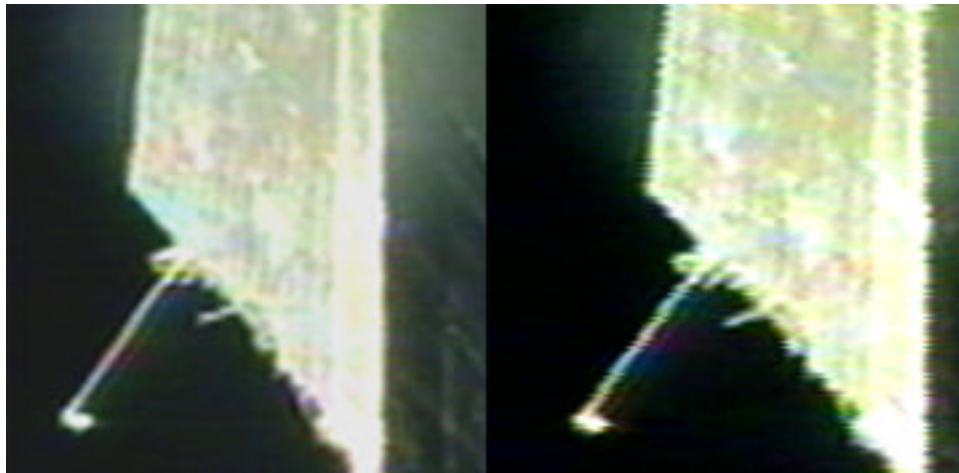


**Figure 5.2 An Example of Acceptable (left) and Unacceptable
(Pixel Shifted) Video Frames**

Manual extraction of data from the video was then undertaken to determine the motion of the array tip. Alternate frames from thirty seconds of video (450 frames total) were selected and an edge enhancement technique was employed on each frame to facilitate identification of the point being tracked. The location of the point was manually selected for each frame. The uncertainty in selecting the same position on the array for each frame analyzed was estimated to be \pm one inch.

Standard photogrammetric techniques were used to determine the location of the point in Shuttle coordinates. Several data inputs are required for the photogrammetry software. These include the image coordinates of the point being tracked for each frame, the image coordinates and object space coordinates of control points, and the object space coordinates of the cameras.

The coordinates of known points on the Docking Module were used for determination of the orientation angles (pointing directions) and effective focal lengths of the cameras. The photogrammetry software computed, for each video frame, the Shuttle coordinates for the point being tracked.

5.3 Results: Motion Analysis of Kvant-2 Solar Panel #2

In order to smooth the noise due to fluctuations in placement of data points, a moving average of the deflection data was calculated over 15 frames (1 second). These results are shown in Figures 5.3 and 5.4 for the out-of-plane and in-plane motions as a function of time. The peak-to-peak deflections were approximated from these smoothed curves as 1.3 inches (3 pixels) for out-of-plane motion and 2.2 inches (4 pixels) for in-plane motion. Due to the noise in the data, a Fast Fourier Transform (FFT) was applied to determine the dominant frequency. The graphs of the FFT's for the out-of-plane and in-plane data are shown in Figures 5.5 and 5.6. To emphasize the frequency of the motion and remove the frequency data associated with the sampling rate of the data, a small section of the fourier transformed data is plotted. The dominant frequency for both the in-plane and out-of-plane motion is approximately 0.4 Hz. The structural model predicts frequencies at approximately 0.15 and 0.4 Hz. To more accurately determine the amplitude and frequency from video, data with a greater signal-to-noise ratio must be acquired.

Results of the Kvant-2 SP#2 motion analyses have been transmitted to the MiSDE principal investigator for structural dynamics analyses. Further video analyses are being performed to measure the motion of Base Block SP#2 in response to the three Shuttle thruster firing sequences.

5.4 Recommendations

The following recommendations are made for future MiSDE solar array motion acquisition:

- The PLB camera field-of-view should be smaller to focus on a smaller section of the solar array. The amplitude of the array motion would then span more pixels in the video frame. Small amplitudes could then be easily measured as they would show up as motion over a range of several pixels.
- IRIG timing must be recorded onto the tapes which contain the video.
- The allocated time for the crew to perform set-up of the cameras must be scheduled during a day pass.

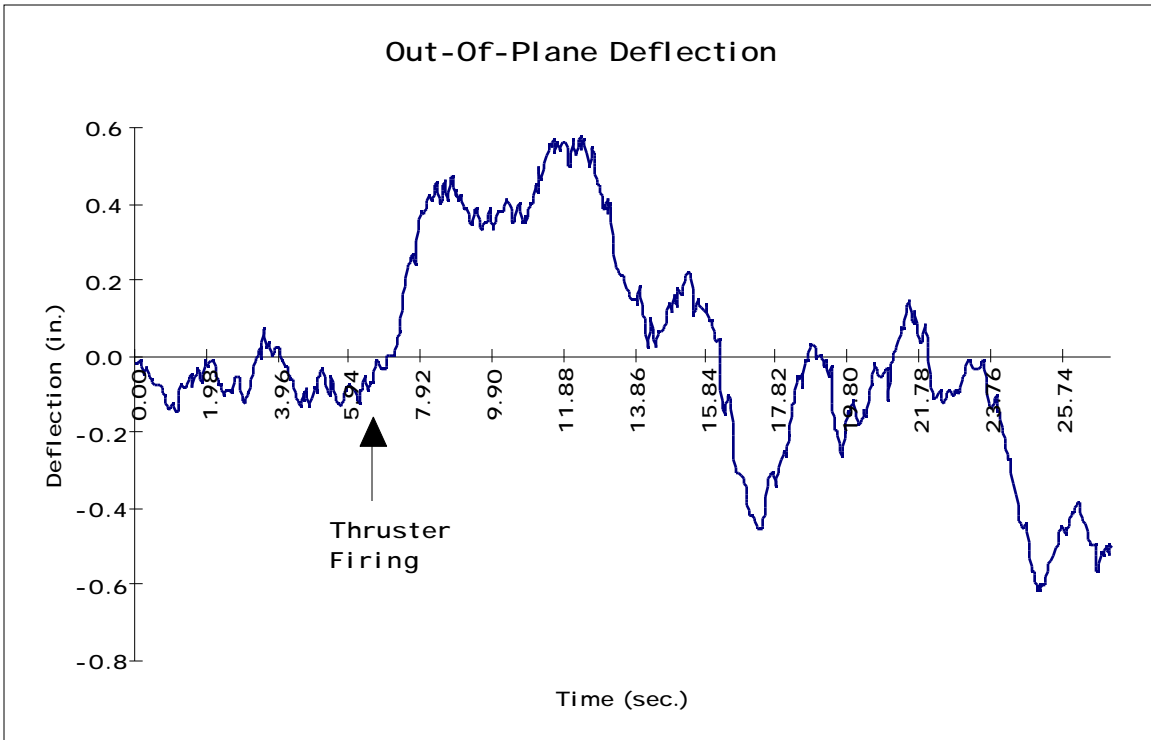


Figure 5.3 Out-Of-Plane Deflection of Kvant-2 SP#2

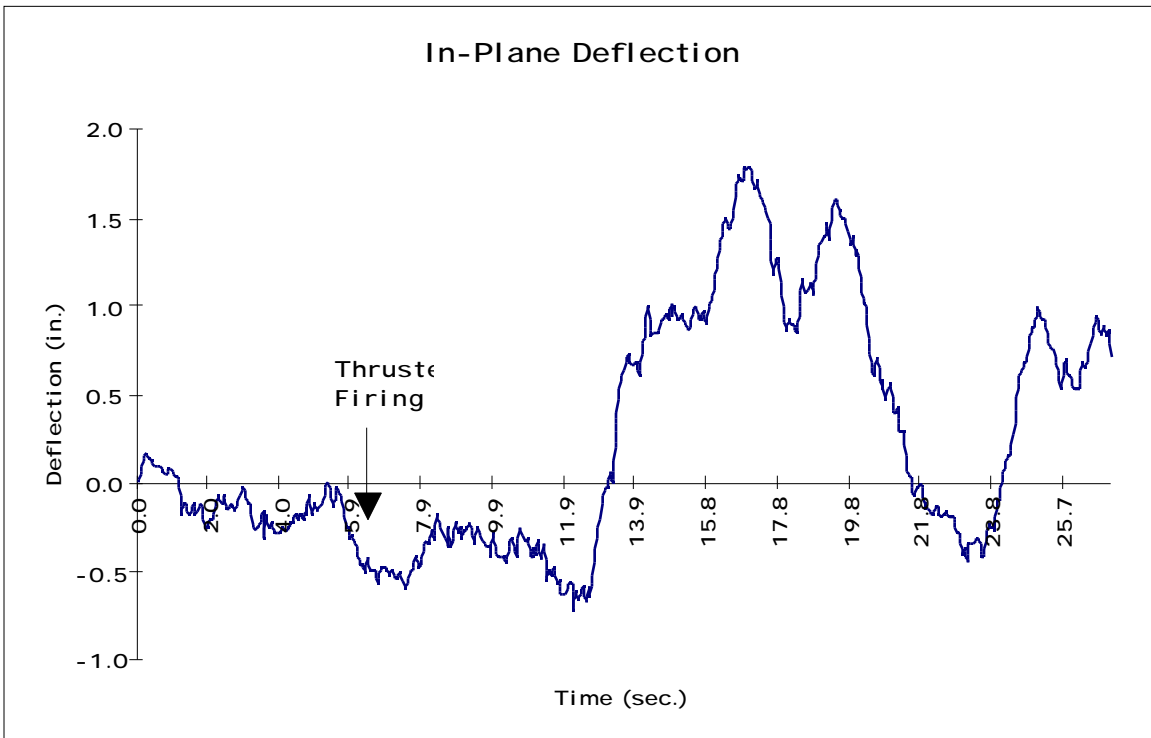


Figure 5.4 In-Plane Deflection of Kvant-2 SP#2

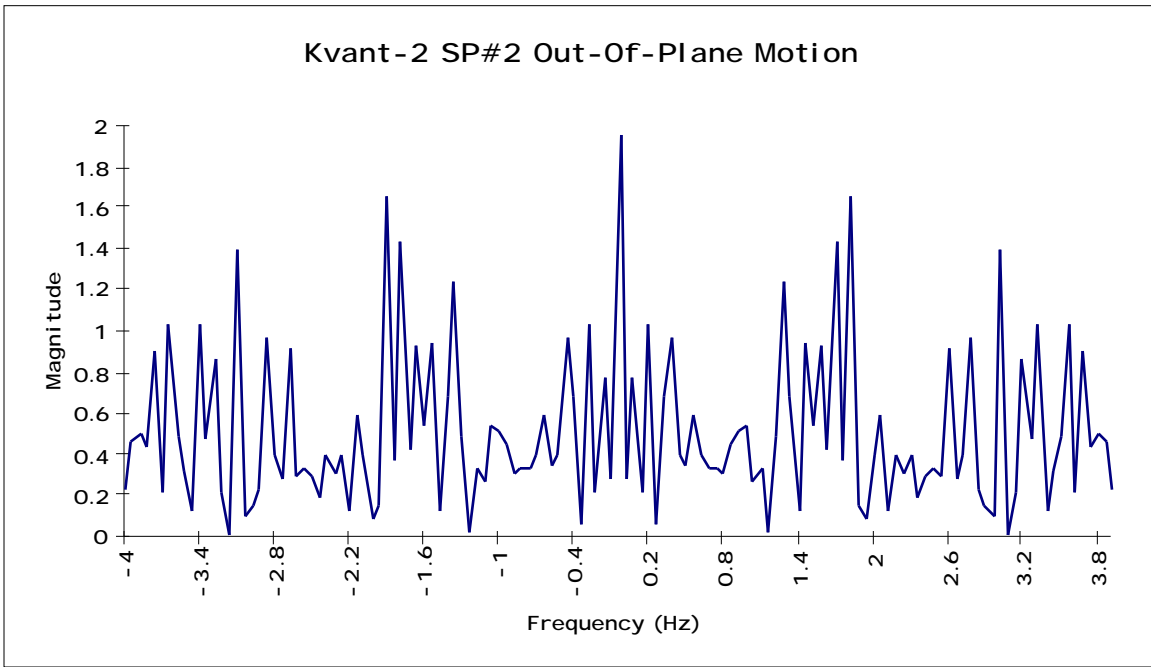


Figure 5.5 Fourier Transform Results for Out-of-Plane Deflection for Kvant-2 SP#2

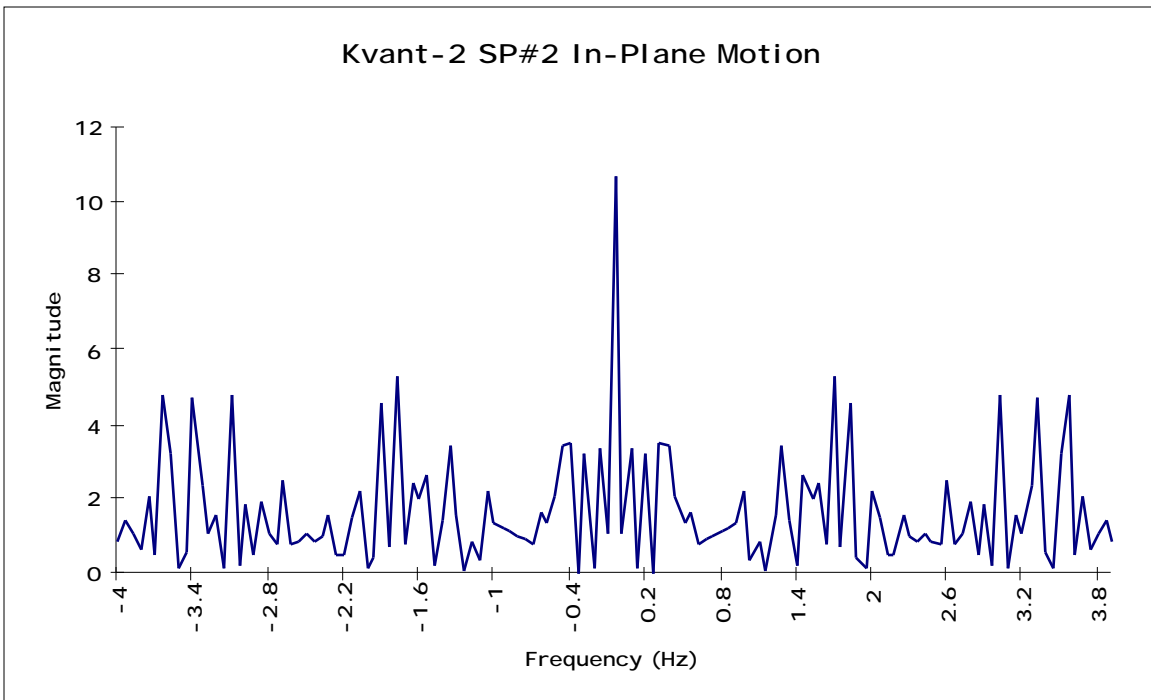


Figure 5.6 Fourier Transform Results for In-Plane Deflection of Kvant-2 SP#2

6. DEBRIS DURING DOCKING OPERATIONS

Small pieces of debris are seen on orbit during most Shuttle missions. Three general origins of these small debris were observed in STS-81 video images during the Orbiter docking sequence. The three origins are: (1) debris originating from the ODS and Docking Module interface area at soft dock, (2) debris originating from within the Orbiter Payload Bay, and (3) debris observed within the confines of the ODS. None of the debris is observed to impact Mir. All of the debris is small and does not exhibit identifiable features.

STS-81 video showed only a few pieces of debris before the time of soft docking. The final approach to docking was performed with illumination by payload bay (PLB) and docking lights and without solar illumination. Debris is significantly more visible when it is sunlit.

Directions of representative debris originating from the payload bay and from the DM/ODS interface area are shown in Figure 6.1. The debris was observed with PLB Camera D between GMT 015:03:55:14 and 03:56:43. Some of the debris appears to be tumbling, with a “flat” side, and hence is visible only on intermittent frames. Despite their apparent proximity to the Mir, none of the debris is seen impact the Station.

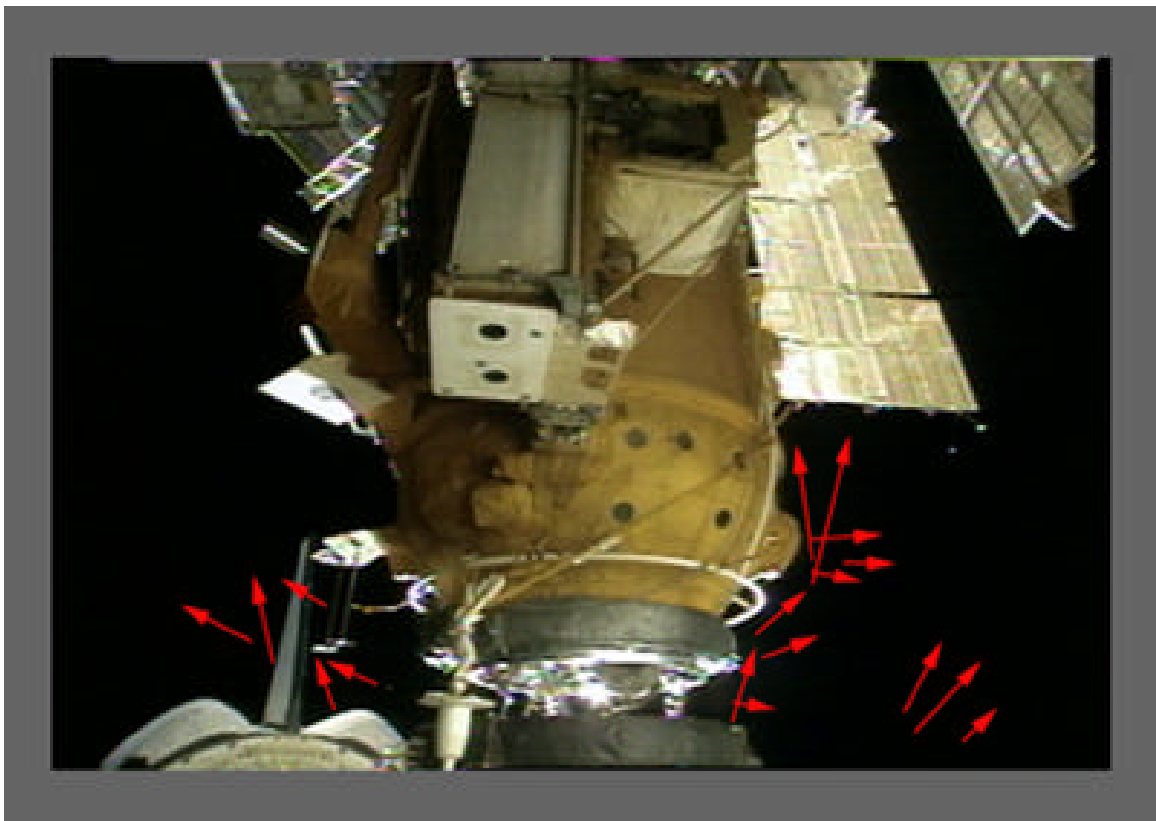


Figure 6.1 Trajectories of Small Debris Observed during Soft Dock

Although Camera A was directed toward the ODS/DM interface, extensive glare and internal reflections degraded the available imagery. However, two pieces of small debris were simultaneously detected with Camera A as shown in Figure 6.2. This debris was

observed at approximately 20 seconds after soft dock. In this figure, item A originates from the lower left of the camera field-of-view and traverses an irregular path until it makes contact with and adheres to the Camera A lens in the position shown. This piece of debris appears circular in the image and is adjacent to another unidentified feature on the lens. The unidentified feature is just to the lower right of the debris in Figure 6.2. The second piece of debris, item B, shows a single piece of debris which traverses in a direction such as to have possibly originated from Mir as indicated by the arrow. There is no observed impact of debris item B.

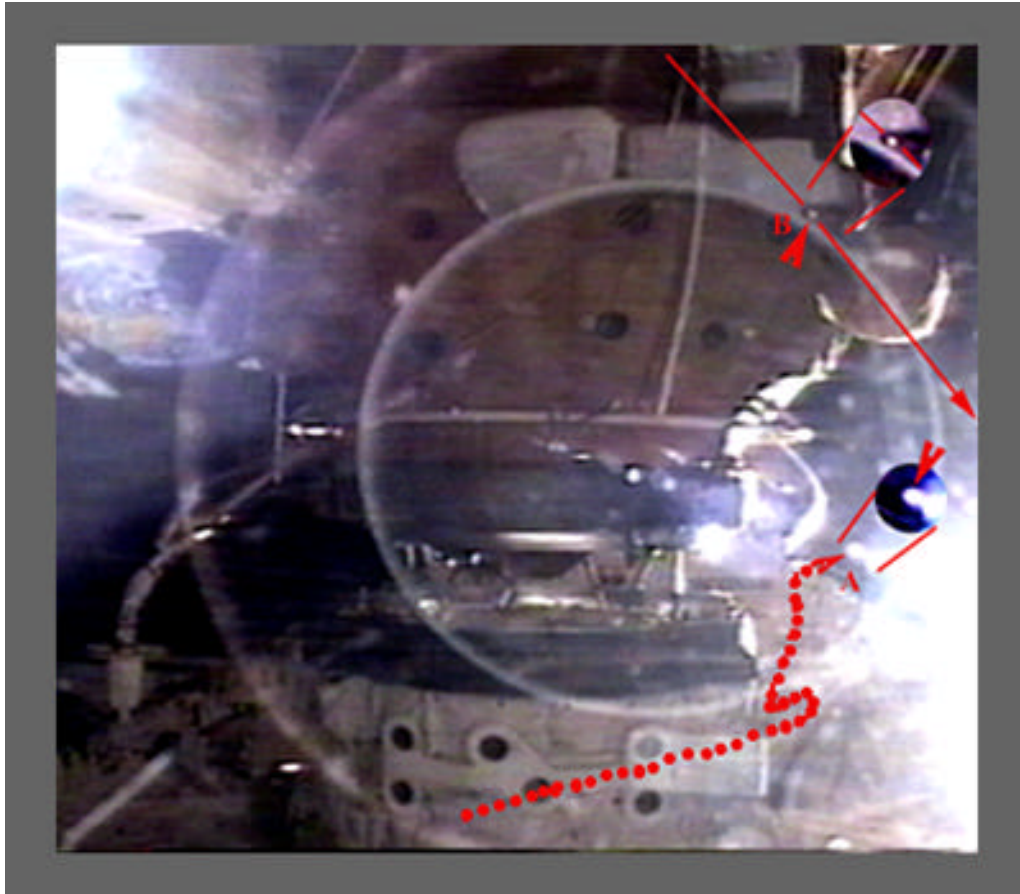


Figure 6.2 Debris Observed in Payload Bay Area during Soft Dock

Also, at the time of docking, several pieces of small debris were observed within the confines of the ODS by the ODS centerline TV (CLTV) camera. Figure 6.3 is a composite image which shows two of these pieces of debris, which appear to be of different origin and composition. A ring-shaped debris traverses from upper-left to lower-right as indicated by the arrow. The video shows this ring-shaped debris traverses between the ODS CLTV camera and the target alignment wire within the ODS. Several other less prominent ring-shaped debris traverse in a similar direction as shown by the arrow C. The second debris, item B, does not appear to be ring-shaped and traverses in a direction from bottom to top in Figure 6.3. Other debris of similar appearance also traverse in a similar direction as indicated by the arrow D.

The image in Figure 6.4 was taken by the centerline camera in the same time-frame (soft-dock) as the images in Figures 6.1, 6.2, and 6.3. Figure 6.4 shows an enhanced version of a part of one video frame which appears to indicate a debris impact and disintegration. Because the debris appears in only one frame, and there was no indicated effect on the target backplate, the apparent impact may have been on the lens surface rather than the target surface.

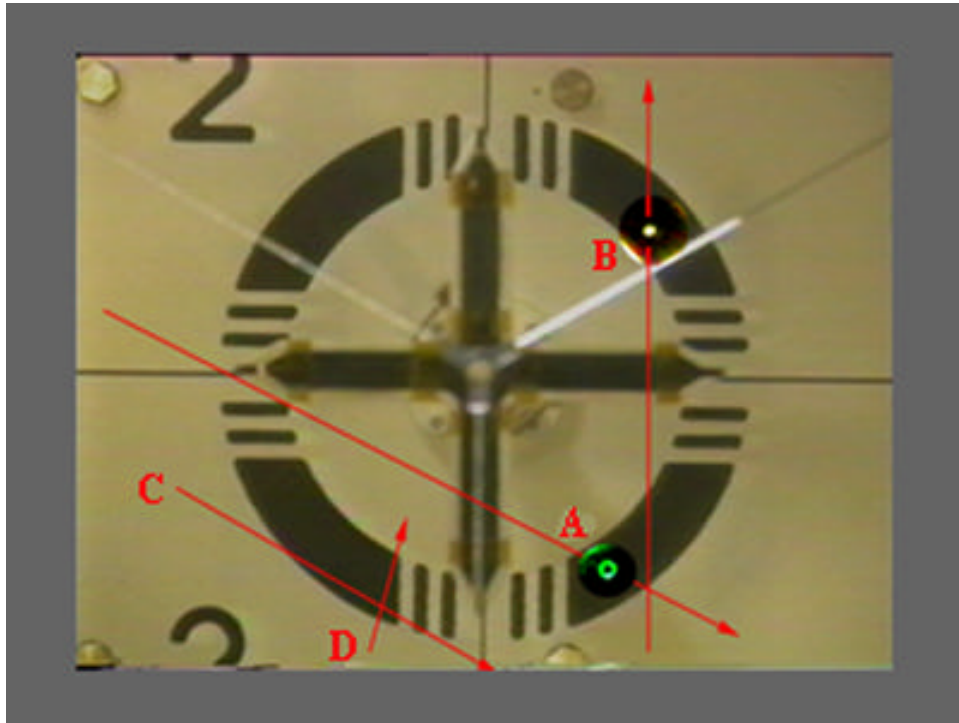


Figure 6.3 Debris Observed Internal to ODS during Soft Dock

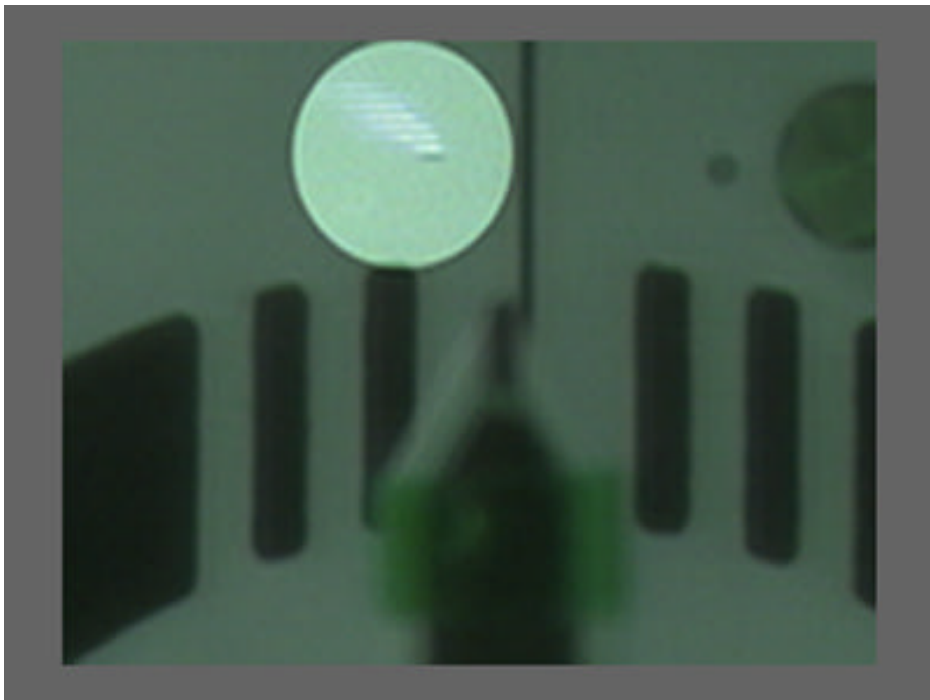


Figure 6.4 Apparent Debris Impact and Disintegration

7. MIR ENVIRONMENTAL EFFECTS PAYLOAD ASSESSMENT

The Mir Environmental Effects Payload (MEEP) experiments were attached to the Mir Docking Module during STS-76. MEEP is composed of four separate experiments: The Polished Plate Micrometeoroid and Debris (PPMD) experiment, the Orbital Debris Collector (ODC), and the Passive Optical Sample Assemblies (POSA and POSA II). The purpose of the MEEP experiments is to study the frequency and effects of space debris striking the Mir Space Station. The MEEP panels also expose selected and proposed International Space Station (ISS) materials to the effects of space and orbital debris. Because ISS will be placed in a similar orbit to Mir, MEEP will give engineers an opportunity to test materials for the ISS in a comparable orbital environment. Imagery of the MEEP panels is acquired on each Shuttle rendezvous mission and that imagery is analyzed for changes to the MEEP panels. Figure 7.1 is an image of the Docking Module with MEEP experiments identified.

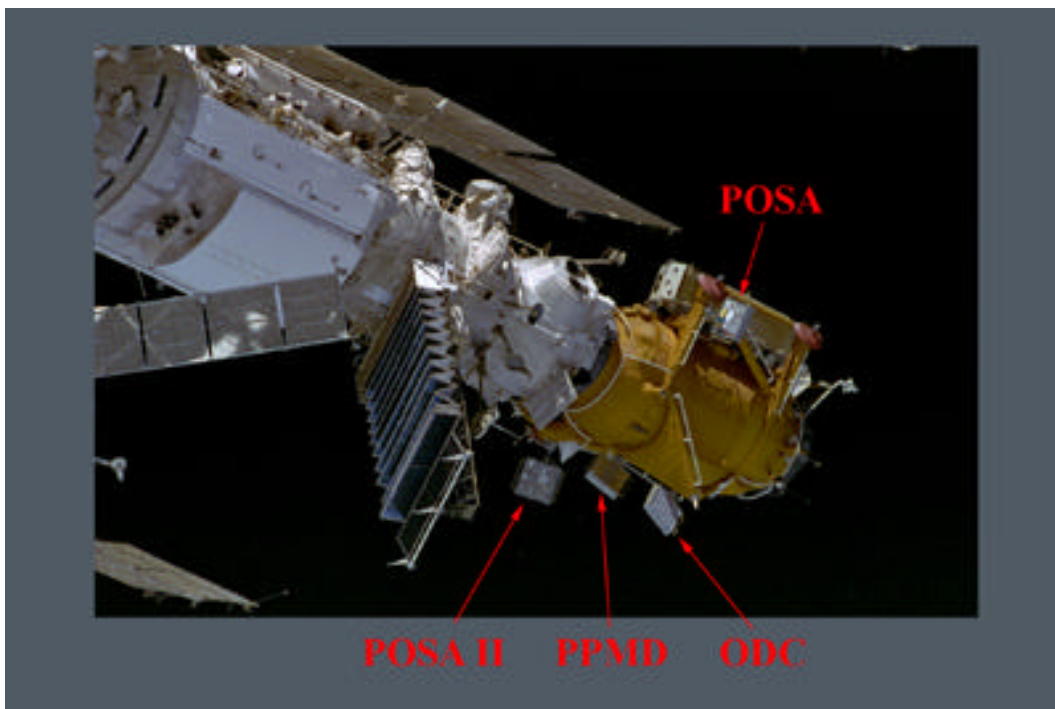


Figure 7.1 STS-81 Image of Mir with MEEP Experiments

Imagery was acquired of MEEP from five vantage points during STS-81. This imagery included still photography of the Docking Module and MEEP experiments during Station-keep, still photography from the Shuttle aft flight deck window while Shuttle was docked to Mir, PLB video surveys while Shuttle was docked, still photography during the back-away of the Shuttle, and still photography acquired during the fly-around of the Mir by the Shuttle.

The orientation of the POSA panel is such that high-quality imagery can be obtained during approach with long focal length lenses and with both still cameras and video while the

Shuttle is docked to Mir. The video images from PLB camera D, and still photographs from the Shuttle aft flight deck window, are sufficient to show no significant damage or discoloration on the Shuttle facing panel of POSA. Figure 7.2 shows an image of POSA taken with the PLB Camera D during the video survey.

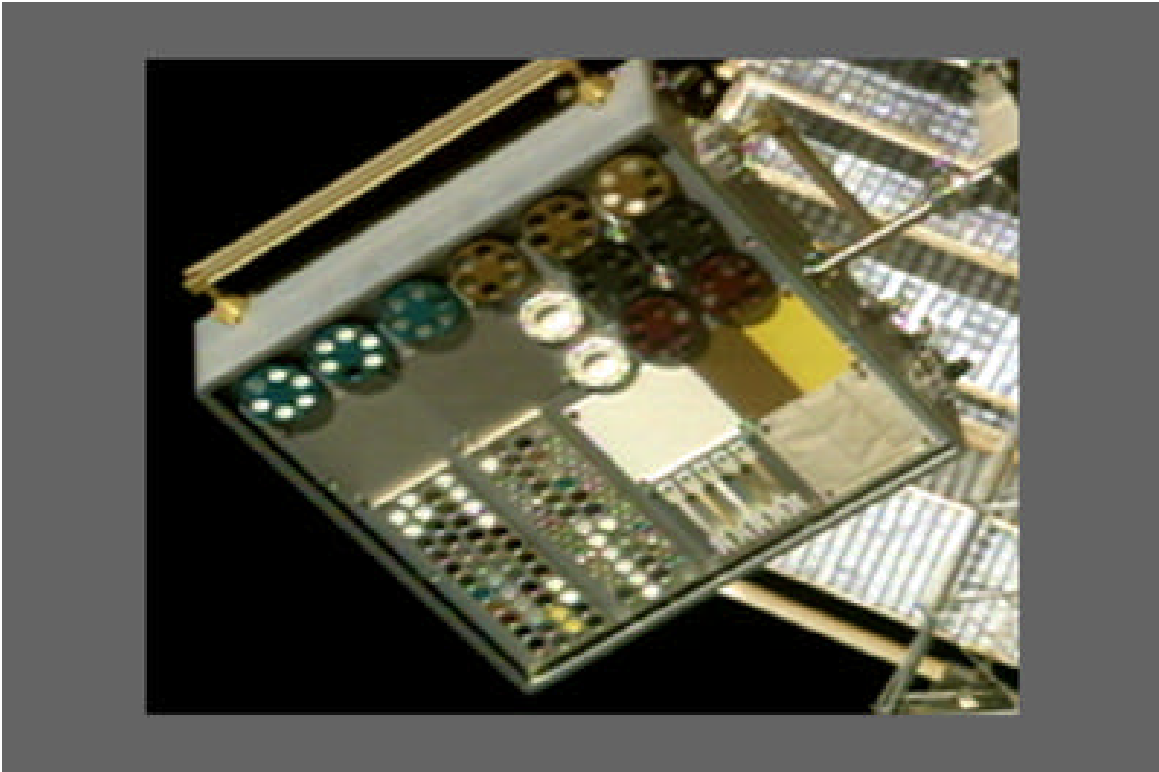


Figure 7.2 Video Image of POSA Front Panel

Figure 7.3 shows both the front panel of POSA II as obtained during approach and the back panel as obtained during the fly-around. Both views are digitally enlarged and contrast enhanced. The back panel view was extracted from the Figure 7.1. No significant damage or discoloration to either POSA II panel is detectable.

Figure 7.4 shows the back panels of POSA, PPMD, and ODC as extracted from Figure 7.1. The POSA view is face-on and no damage or discoloration is discerned. The ODC image, although oblique, is of good quality and no damage or discoloration is indicated. The imagery of PPMD also does not indicate damage or discoloration. However the polished metallic surfaces have substantial reflections of Mir which could mask potential discoloration.

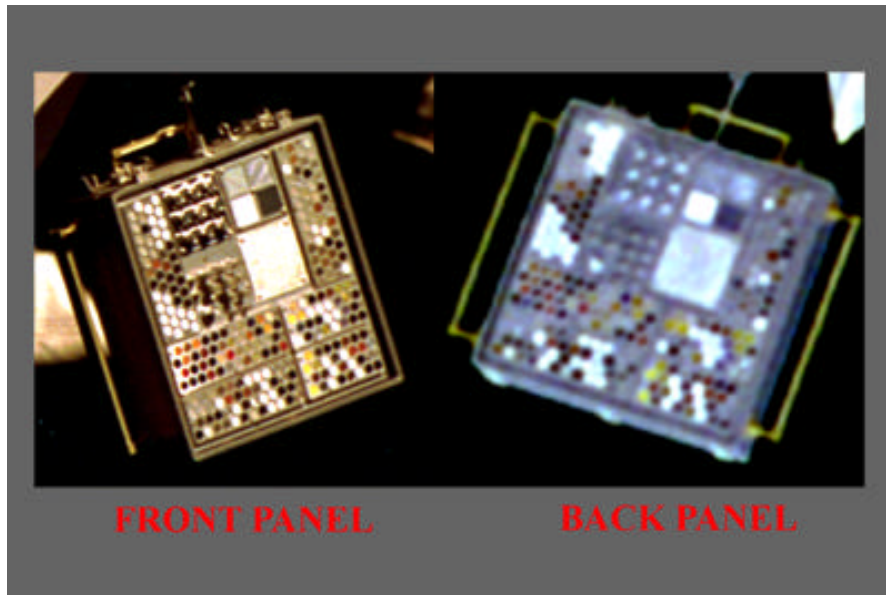


Figure 7.3 Still Photographs of POSA II Front and Back Panels

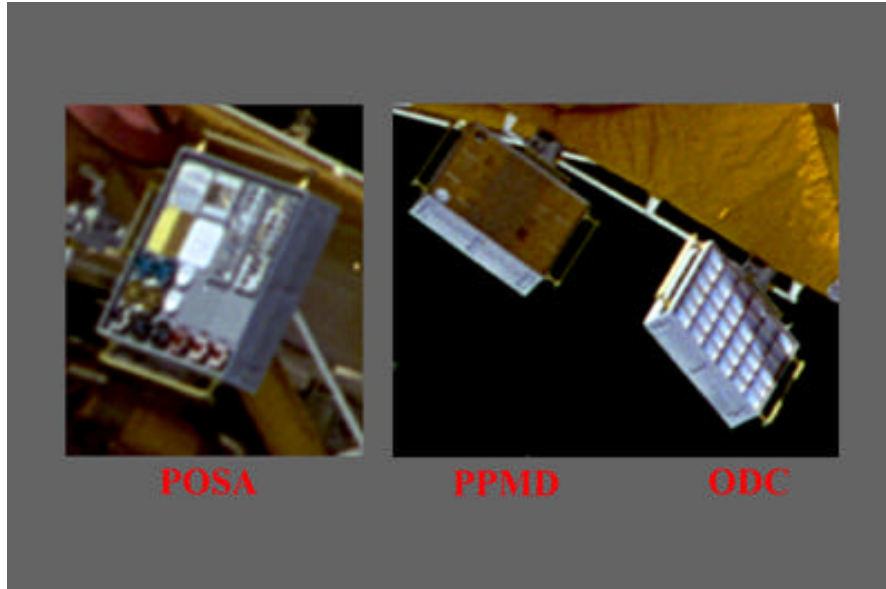


Figure 7.4 Still Photographs of POSA, PPMD, and ODC Back Panels

Table 8-1 is a list of the requested analysis events and corresponding times. The availability of video for the requested times is also listed. The available frames of video were located on digital tape, captured to digital disk, and uploaded to a computer. An image processing software package was used to measure points in the chosen frames of video.

Table 8-1 Analysis Cases and Video Availability

Event	GMT (ddd:hh:mm:ss:fr)	Centerline video?	Non-axial video?
Pre-flyout	015:03:48:00:00	yes	no
Post-flyout	015:03:50:00:00	yes	no
Pre-contact 1	015:03:54:45:04	yes	no
Pre-contact 2	015:03:54:48:11	yes	no
Post-contact	015:03:55:23:29	yes	yes
Pre-separation 1	019:14:52:35:00	no	no
Pre-separation 2	019:01:57:42:21	yes	yes
Undocking	020:01:56:56:00	no	yes

8.1 Determination of Position and Roll of Centerline Camera Relative to the ODS

Positional misalignment of the centerline camera was determined from a frame of video captured during the Shuttle's approach to Mir. Figure 8.2 shows this frame of video with the Mir omitted for clarity. The alignment guides of the ODS and the alignment washer are seen in this frame of video. The alignment washer is a small object at the intersection of supporting wires which extend from the petals. Three steps were taken to determine the offset of the centerline camera and alignment washer in relation to the center of the ODS.

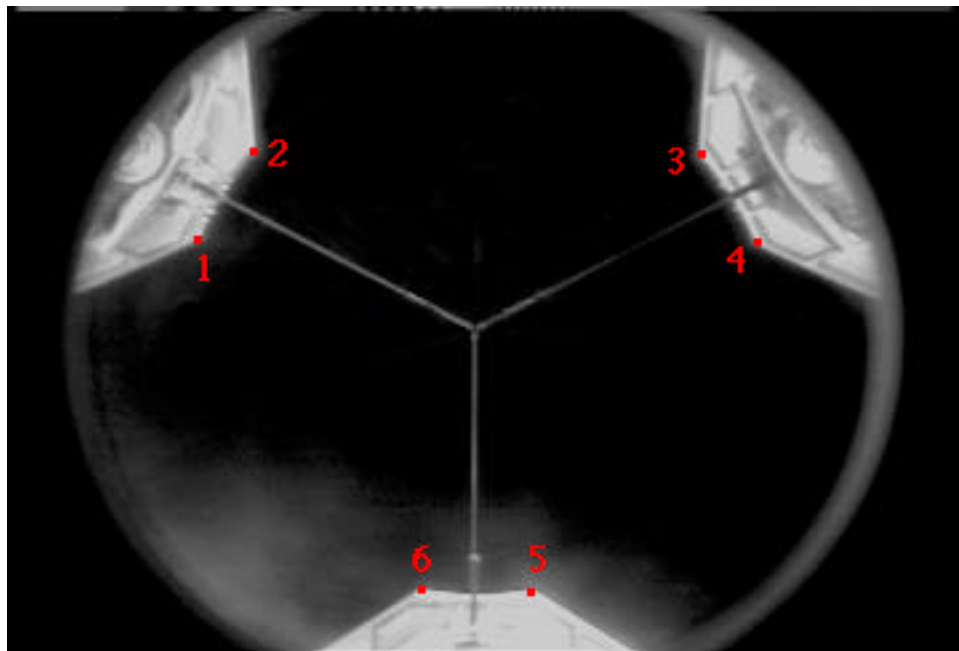


Figure 8.2 ODS Features Used in Alignment Analysis

First, the optical axis of the centerline camera was determined by assuming that the center of the frame of captured video was the optical center of the camera. The midpoint of the frame could then be computed from a known image size of 646 x 486 pixels.

Second, the center of the alignment washer assembly was determined. Points along the wires were chosen to define lines in the image space that correspond to the wires supporting the alignment washer. The intersections of these lines were then determined. Due to small measurement errors, the three lines did not intersect at a single point. The average value was used as the center of the alignment washer assembly.

Third, the center axis of the ODS in relation to the frame of video was determined. As the alignment guides divide the circular ODS into equal sections, they were used in the determination of the center axis of the ODS. Points at both tips of each ODS alignment guide were chosen (see Figure 8.2). From the points 1 to 6, a circle and its center were determined using a commercial software package (MATLAB). Using the radius from the center axis of the ODS to a tip on an ODS petal for scale, the differences between the ODS axis and the camera optical axis (video frame center) were determined. The computed ODS center minus the video frame center was computed to be $\Delta X_o = 0.00 \pm 0.07$ and $\Delta Y_o = -0.39 \pm 0.07$ inches in Orbiter Structural Coordinates. The computed alignment washer center minus the video frame center was computed to be $\Delta X_o = 0.00 \pm 0.08$ inches, $\Delta Y_o = 0.54 \pm 0.08$ inches. Figure 8.3 shows the locations of the computed centers. An uncertainty of ± 1 pixel in point placement is used to estimate the error.

In addition to the positional misalignment, the rotational misalignment (roll) of the centerline camera was calculated from the view shown in Figure 8.2. Points 1 through 6 were used to define parallel lines in the image by creating line segments from points 2-3, 1-4, and 5-6. If the centerline camera shows no rotational misalignment, these lines will be perfectly parallel to the X-axis of the image. This was not the case for STS-81. The X and Y intercepts of these parallel lines were determined, and the angles between these parallel lines and the X-axis of the image were used to determine the roll of the camera. Three measurements were made using the six tips of the ODS petals resulting in an average camera roll of $-0.38^\circ \pm 0.25^\circ$ in Shuttle Dynamic Body Coordinates (the coordinate system in which yaw, pitch, and roll are provided to the crew). The dominant contribution to the standard error in this result is the mounting tolerance ($\pm 0.25^\circ$) between the ODS base and the Shuttle Androgynous Peripheral Docking Unit (APDU) alignment guide ring to which the petals are attached. The standard error due to image measurements is ± 0.02 .

8.2 Determination of Indicated Roll of the Centerline Camera

Because the centerline and non-axial cameras are oriented in the -Z direction of the Shuttle, any roll in the alignment of the camera would be reflected as a need for a relative yaw correction for the Shuttle. Therefore, the relative yaw correction is equivalent to an indicated roll in the centerline camera.

Pre- and Post-flyout

The only available views at pre- and post-flyout containing centerline camera video were muxed with PLB Camera D. As such, the middle 50% of the unmuxed video view was present in the muxed view, i.e., one-quarter of the video frame was removed from the left and right sides. From the muxed view of the centerline target, the angular displacement of the roll markers on the backplate from 90° was measured. This was accomplished by measuring the location of the side of a roll marker at the top and bottom of the video frame. The difference in edge locations determines the yaw of the Shuttle according to the centerline camera. This yaw value measured $0.8^\circ \pm 0.4^\circ$ at pre-flyout and $-0.8^\circ \pm 0.3^\circ$ at

post-flyout in Shuttle Dynamic Body Coordinates. (The difference between the error values are due to different resolutions in the pre- and post-flyout images.)

Indicated Camera Roll at Contact

At contact, the same method used to determine Shuttle yaw during pre- and post-flyout was used to determine centerline camera roll. Specifically, the angular displacement of the yaw markers on the backplate from 90° was measured. This was accomplished by measuring the location of the side of a yaw marker at the top and bottom of the video frame. The difference in edge locations determines the indicated roll of the camera. This value for the centerline camera is $0.3^\circ \pm 0.1^\circ$ and is $0.3^\circ \pm 0.1^\circ$ for the non-axial camera at contact.

Indicated Camera Roll at Pre-separation

A second measurement was made to determine the indicated roll of the camera prior to separation. The indicated roll of the non-axial camera was also determined. The same method described above was used to determine the values. At pre-separation, the indicated roll of the centerline camera measured $-0.1^\circ \pm 0.1^\circ$ and the non-axial camera indicated roll measured $0.3^\circ \pm 0.1^\circ$.

Note that the indicated roll of the centerline camera changes (improved) from contact to pre-separation. However the indicated roll of the non-axial camera does not change. This difference may be attributed to the fact that the centerline camera must be removed before the Shuttle crew can enter the Mir. Before undocking, it is replaced. This removal and replacement may be relevant to the differences in indicated camera alignment between docking and pre-separation.

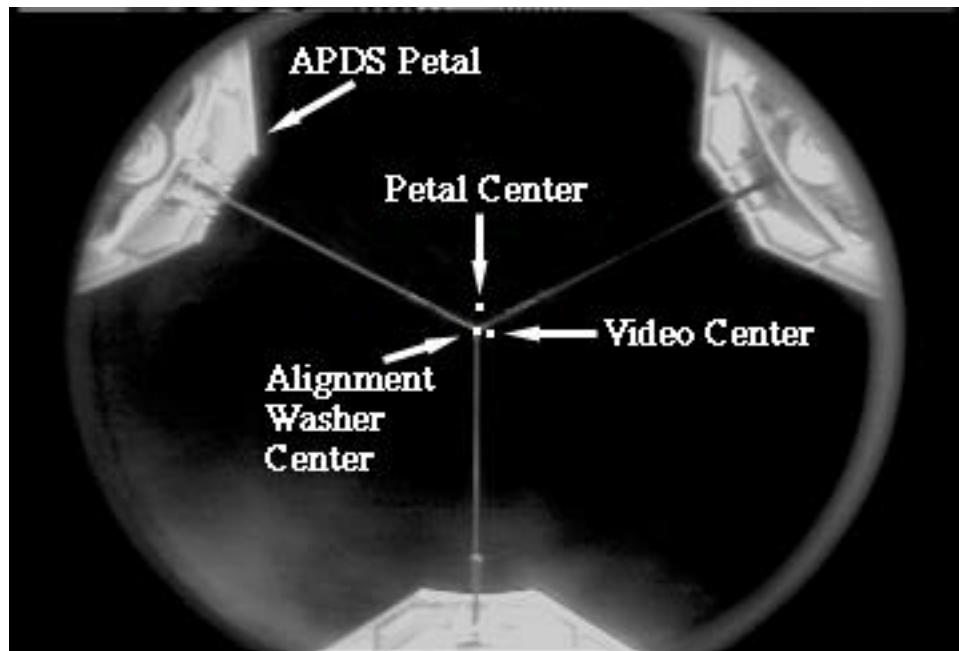


Figure 8.3 The Relative Centers of the ODS as Computed from the Alignment Guides, the Video Frame, and the Alignment Washers

Alignment of Stand-off Target Relative to Backplate at Contact

At contact, points along the edges of the stand-off target and degree markers were measured to determine the center-lines of the stand-off cross and backplate. The two lines between the edges of the center degree markers at the top and bottom were determined and a center-line between these two was determined. Similarly, a center-line was determined for the vertically oriented stand-off target arms. The angular misalignment was computed as the angle formed by the two center-lines. The distance between the degree markers provided scale. It was assumed that, at contact, the interface planes of the ODS and Docking Module on the Mir were parallel. The yaw marker values were measured at the top and bottom of the video frame and the two values were averaged. The same procedure was repeated for the non-axial camera. The misalignment (backplate minus stand-off target) was computed as $-0.35^\circ \pm 0.08^\circ$. The non-axial camera showed a misalignment of $-0.17^\circ \pm 0.09^\circ$. (Negative misalignment is measured for the target cross being rotated counter-clockwise relative to the backplate.)

Alignment of Stand-off Target Relative to Backplate at Pre-separation

The same procedure that was used in measuring the alignment of stand-off target at contact was used for measuring the alignment prior to separation. The misalignment of the target before separation is estimated as $-0.16^\circ \pm 0.06^\circ$. The non-axial target misalignment error is estimated as $-0.28^\circ \pm 0.09^\circ$ in Shuttle Dynamic Body Coordinates.

Note that video recorded prior to undocking shows a different value for target/backplate alignment than was determined at contact. This difference may be attributed to the fact that the centerline camera, alignment washer, and Docking Module stand-off cross must be removed before the Shuttle crew can enter the Mir. Before undocking, they are replaced. On STS-81, a new stand-off cross was installed before undocking. This removal and replacement may be relevant to the differences in indicated camera alignment between docking and pre-separation. The previous stand-off cross could have been slightly bent, the new cross could have a slight bend, the centerline camera was centered about its optical axis when replaced, or any combination of the three.

8.3 Results

Positional misalignment of the centerline camera was measured to be $Y_o = -0.39 \pm 0.07$ inches in Shuttle Structural Coordinates prior to docking. This offset could also be explained by an angular offset from the optical axis of the camera. A combination of these misalignments is the likely cause, but the degree of positional versus angular misalignment can not be determined due to a lack of adequate features in the video. Rotational misalignment (roll about optical axis) was measured as $-0.38^\circ \pm 0.25^\circ$ in Shuttle Dynamic Body Coordinates. The indicated camera roll results from this analysis are presented in Table 8-2. Cells marked with an asterisk (*) denote a requested measurement for which no calculations were made because the applicable video was not acquired.

Table 8-2 Camera Indicated Roll Relative to Mir

Event	Centerline Roll	Non-axial Roll
Pre-flyout	$0.8^\circ \pm 0.4^\circ$	*
Post-flyout	$-0.8^\circ \pm 0.3^\circ$	*
Contact	$0.3^\circ \pm 0.1^\circ$	$0.3^\circ \pm 0.1^\circ$
Pre-separation	$-0.1^\circ \pm 0.1^\circ$	$0.3^\circ \pm 0.1^\circ$

Based on the results, the following are observed:

- There was a positional and rotational misalignment of the centerline camera on STS-81 prior to docking. There was no applicable video obtained to determine a comparable alignment after the centerline camera was replaced i.e., during pre-separation or backaway.
- The indicated pre- and post-flyout centerline roll values are equal in magnitude, but different in sign.
- The centerline camera alignment improves from Shuttle contact to pre-separation.
- The non-axial camera alignment does not change from Shuttle contact to pre-separation.
- There is a misalignment between the stand-off cross and the target backplate.

The improvement in indicated centerline camera alignment from contact to pre-separation suggests that removal and replacement of the centerline camera and stand-off cross has a marked effect on the perceived alignment of the Shuttle.

9. POSITION OF THE NEW KURS ANTENNA ATTACHED TO THE DOCKING MODULE

Between STS-79 and STS-81, a Kurs antenna was attached to the Mir Docking Module. This Kurs antenna extends toward the Shuttle forward bulkhead as shown in Figure 9.1. The JSC Structures and Mechanics Division requested that an analysis be performed to determine the position of the tip of the antenna. This information will assist the group in determining the flight clearances between the antenna and the Shuttle Payload Bay forward bulkhead.

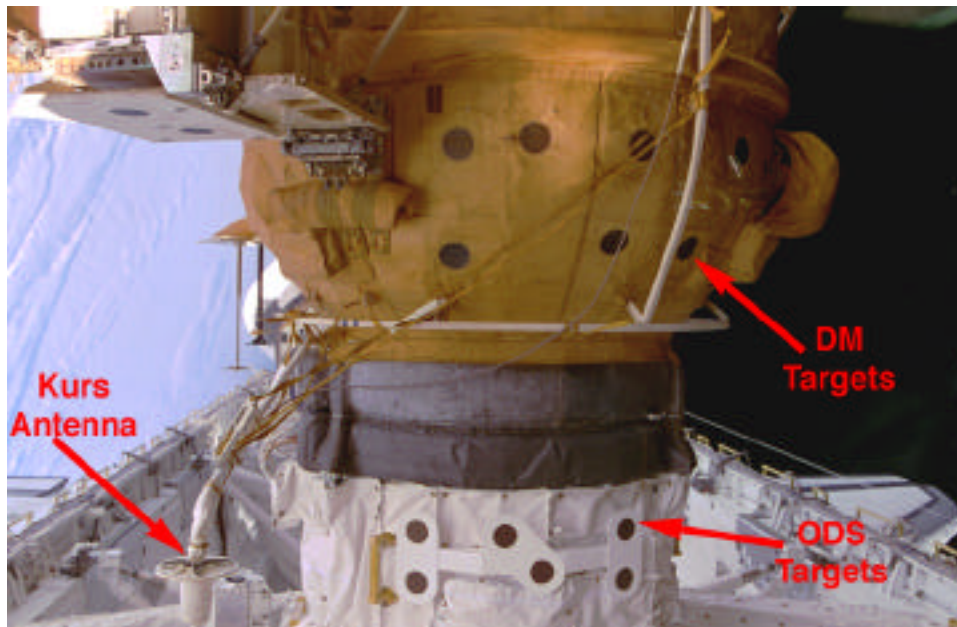


Figure 9.1 Kurs Antenna as seen from the Shuttle Flight Deck on STS-81

Standard photogrammetric techniques were used to determine the location of the Kurs antenna. Two overlapping images of the antenna were used to perform three-dimensional intersections of image rays, the intersection being the tip of the Kurs antenna. Image points of objects of known locations are used to establish the relationship between image space and object space, and allows the determination of the position of the antenna in the Shuttle Structural Coordinate System (SSCS). These objects of known location are the Orbiter Space Vision System (OSVS) targets labeled as DM targets and ODS targets in Figure 9.1.

Two STS-81 video images from Shuttle PLB Cameras A and D were used in this analysis. These two images are shown as Figures 9.2 and 9.3. The image coordinates of targets ODS1 through ODS6 on the ODS were determined in both images. Image coordinates were also obtained for Docking Module targets TB7 and TB8 in the video image from camera A. Other OSVS targets were not utilized due to shadows in the field-of-view. A centroid analysis of the image pixels corresponding to each OSVS target was performed to determine the image coordinates of the targets. The color video frames were first converted into grayscale images, and then binarized to perform centroid analysis on each target more precisely.

The image coordinates of the Kurs antenna tip were also determined for the two video frames. Edge enhancement techniques were employed to precisely identify the tip of the antenna.

The location of the Kurs antenna tip in SSCS coordinates during STS-81 is: $X_0 = 685.5 \pm 1.9$, $Y_0 = 42.3 \pm 1.1$, $Z_0 = 439.3 \pm 0.9$ inches. The errors are 3σ values. These coordinates show a clearance of 109 inches between the tip of the antenna and the Shuttle forward bulkhead on STS-81. The expected coordinates based on data obtained from the Space Shuttle Program Integration Engineering Office are $X_0 = 683.4$ inches, $Y_0 = 40.5$ inches, $Z_0 = 439.1$ inches.

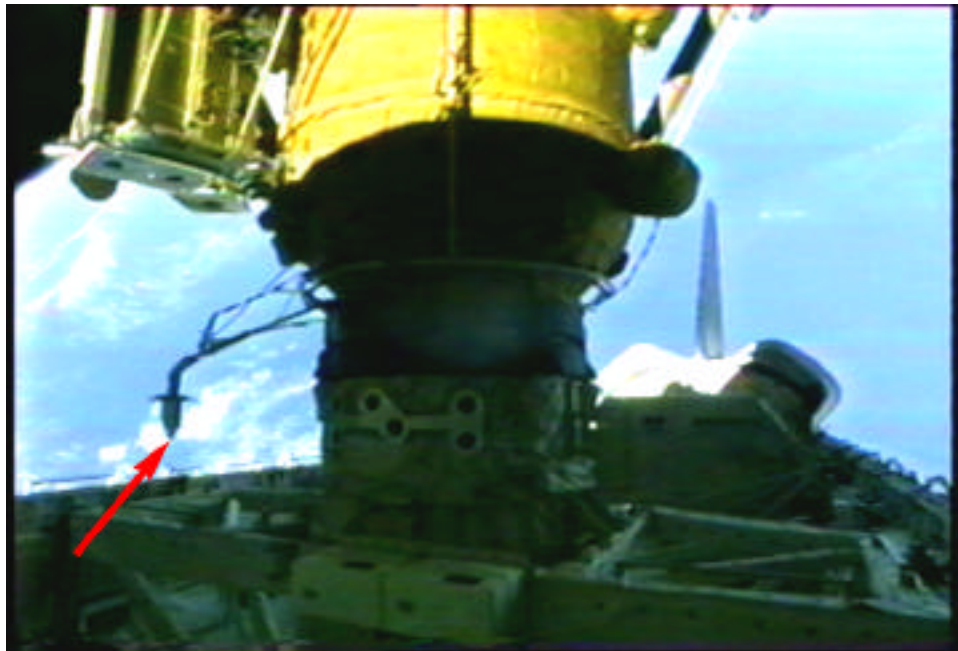


Figure 9.2 Kurs Antenna as seen from Payload Bay Camera A

The errors in the location of the Kurs Antenna were determined based on the estimated operator errors in locating the image coordinates of the reference points, as well as estimated errors in the location, orientation, and focal length of each camera. The input errors are estimates based on extensive analyses and experience associated with determining positions of features during the Hubble Space Telescope Servicing mission. The determination of output errors was achieved by assuming the errors to be normally distributed and applying a Monte Carlo simulation of 120 iterations.

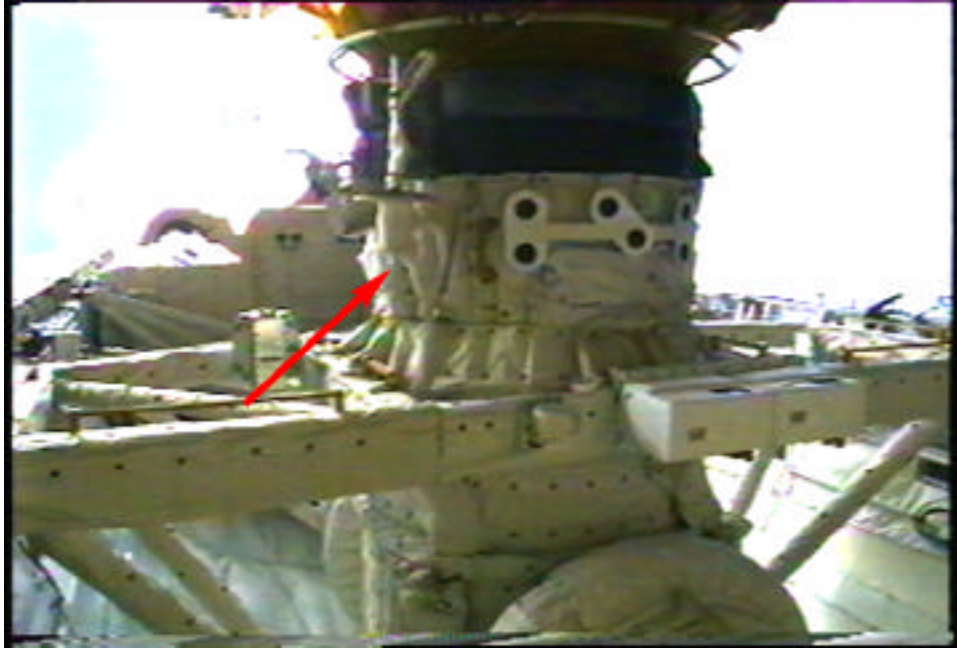


Figure 9.3 Kurs Antenna as seen from Payload Bay Camera D

10. IMAGERY EVALUATION

This section discusses the overall quality of the film and video data obtained during STS-81 for DTO-1118. The scenelist of flight films and an index to videotapes are included as Appendices C and D.

Imagery acquired of Mir surfaces during STS-81 consisted of the following:

- 18 hours of downlink and onboard video.
- 498 frames of 35 mm film.
- 394 frames of 70 mm film.
- 20 Electronic Still Camera (ESC) images.

Included in this video and film are customer requests for coverage of specific targets. All imagery requirements of customers were obtained as well as imagery for other DTO-1118 objectives.

10.1 Video Review

The centerline camera provided the first views of the Mir approximately 1 hour before docking. During the dark phase of the orbit, only the station onboard lights were visible on the available views. The ODS centerline camera provided good viewing of the DM docking ring and the centerline target throughout the docking phase. The centerline imagery is sufficient to show the docking target to be in good condition. However, the imagery detail is not sufficient for assessment of the docking latches or electrical connector mechanisms. PLB Camera D provided clear imagery of the docking, however Camera A had extensive glare at docking.

PLB Camera D provided the only images adequate for monitoring the small debris at docking near the DM and ODS interface. Centerline camera views were used for monitoring small debris internal to the ODS. No identifiable debris was observed during docking.

Much of the downlinked survey video was obtained via INCO ground control during two crew sleep periods of the docked phase. All four PLB cameras were used in acquiring Mir survey imagery. This survey provided good coverage of the Orbiter-facing sides of the Spektr, Kvant-2, Base Block, Kristall, Kvant, and Priroda modules, and the Soyuz and Progress capsules. In addition, systematic coverage of the Docking Module and the attached RSA carrier was obtained.

Detailed video coverage of the RSA revealed peeling paint on different areas of the supporting truss structure. Heavy discoloration was also noted. Coverage of the MEEP panels deployed on the Docking Module was obtained from the payload bay cameras. High quality video was obtained of the POSA panel from PLB camera D. The other three panels were only visible from the aft cameras. The lighting upon the other MEEP panels during the video surveys did not provide for good images of the ODC or PPMD experiments.

The Mir Structural Dynamics Experiment (MiSDE) was performed during the docked phase. During Shuttle thruster firings, PLB Cameras A and D were scheduled to record motion at the tip of Base Block SP#2, while Cameras B and C record motion at the array attach point. During Mir thruster firings, the same camera set-ups were used to record the motion at the tip and attach of the Kvant-2 SP#2 array. However, several problems were

experienced in the acquisition of the required video data of the solar arrays (see Section 5). The allocated time for the crew to perform camera set-up occurred during night passes prior to the test firings. The STS-81 crew commented, during the debrief, that the CTVC payload bay video camera was difficult to set up due to the low light level conditions which preceded MiSDE thruster firing sequences. They could not see enough details in the camera images to align the cameras to optimize the solar arrays in the camera field-of-view. As a direct result, the video of the Base Block array did not occur until after the Shuttle thruster firings had begun. Video obtained during MiSDE test firings on STS-81 was also of insufficient quality for analysis due to a smudge on the PLB Camera A lens. In addition, required timing and camera pointing data was not obtained for all cases.

During the backaway sequence, the centerline camera and the ODS non-axial camera provided views of the Mir docking interface area. The views showed the centerline and non-axial targets to be in good condition. The views, however, are not adequate for assessment of the latches and connectors.

PLB Camera A was used to acquire overview imagery during fly-around. No unusual motion of Mir appendages was noted in this imagery.

10.2 Still Photography Review

STS-81 was the first mission to utilize a 400 mm lens for Shuttle-based imagery of Mir. This lens provided excellent detailed photography during all phases of the flight. The increased level of detail of the 400 mm lens was clearly visible when compared to the 300 mm lens was used during previous missions. Although the crew felt that the restrictive physical dimensions of some of the station windows and the size of the camera equipment made photography from some windows difficult, they nevertheless obtained outstanding high resolution imagery of Mir surfaces using the 400 mm lens.

Approximately 85 frames of Nikon (35 mm) photography was acquired throughout approach. These images were acquired with the 400 and 180 mm lenses, and provided an overview of all Shuttle-facing sides of Mir modules during approach. Imagery of the Docking Module face-on to the docking mechanism was taken with the 35 mm camera and 400 mm lens from a distance of approximately 215 feet prior to the Mir and the Shuttle passing into darkness.

Close-up imagery of the docking mechanism was taken on both approach and backaway with the 35 mm camera and 180 mm lens. This imagery was superior to imagery of the Docking Module docking mechanism obtained previously and definitively showed that all capture and structural latches, alignment guides, docking targets, laser retroreflectors, and electrical connectors were in good physical condition. The images could be enlarged to show specific details and allowed examinations of docking surfaces not previously possible.

Approximately 100 frames of overview fly-around imagery was captured with the 70 mm Hasselblad. Photographs taken with the 70 mm camera provided the best coverage of the +ZB sides of Kvant-2 and Spektr to date. Approximately 85 frames of fly-around photography were also acquired with the 35 mm camera. Early fly-around 35 mm camera photography provided coverage of the -XB sides of Kristall and the Docking Module. The 35 mm camera with the 400 mm lens provided detailed coverage of the +ZB end and -XB side of Priroda, the -YB end and +XB side of Spektr, and the -YB and +XB sides of the Base Block and Kvant. The fly-around photography is the best obtained to date during the Phase 1 program. The combination of good lighting and use of the 400 mm lens on the 35 mm Nikon camera contributed to the excellent fly-around photography. The photographs increase the overall coverage of the external surfaces of Mir while providing the

opportunity to make temporal comparisons between surfaces, such as the -YB sides of the Base Block and Kvant, which have not been photographed since STS-63. Fly-around imagery provided the first detailed imagery of the MEEP panels from the Mir side.

There were 20 Mir-related Electronic Still Camera (ESC) frames taken on this mission. ESC imagery of Mir provided five views of Mir during approach. The other 15 images provided coverage of targets on the surfaces of the Base Block and Spektr.

10.3 Evaluation of 400 mm lens

A focus of imagery evaluation for STS-81 was the image resolution of the new 400 mm lens on the Nikon 35 mm camera. Theoretical analyses have indicated that the 400 mm lens should have about 20 percent higher resolution (line pairs per millimeter) of high contrast targets than the 300 mm lens for equivalent lighting, exposure control, film type and film processing. The scale factor due to the longer focal length should also provide a 25 percent improvement in the minimum resolvable object size for the same camera-to-object distance.

The markers on the backplate of the docking target on the Docking Module provided a facsimile resolution target similar to tri-bar resolution targets used as standards for estimating image resolution. There are both vertical and horizontal three-bar targets on the backplate, referred to as pitch and yaw degree markers (Figure 8.1). These bars are 0.21 inches (5.33 mm) in width and separated by the same distance. By examining imagery on approach, images were found in which these bar targets were barely identifiable. (In the selected images, two diagonally opposite targets were identifiable and the other two targets were not identifiable, thus indicating the threshold of resolution.)

Results indicated a resolution of approximately 22 line pairs per millimeter (lpm). The distance of the STS-81 image was calculated to be approximately 310 feet from the backplate. Based on this distance and using a resolved line pair (0.42 inches or 10.66 mm) as object resolution, the results indicate resolution of an object 10.6 mm in size from a distance of 310 feet. A similar analysis of the 300 mm lens on STS-79 yielded 18 lpm.

The resolution results for the 400 mm lens, when compared to the 300 mm lens, show a strong benefit to manifesting of the 400 mm lens for imagery of Mir and the International Space Station. The 400 mm lens, in conjunction with the 180 mm lens, provide a wide range of capabilities for image acquisition.

Evaluation of the film photography utilized standard production products of third generation positive contact film transparencies, digital images from second generation transparencies, and 8 x 10 inch print enlargements. Original film was not evaluated.

11. CONCLUSIONS AND RECOMMENDATIONS

11.1 Summary

The most significant new anomaly identified from the STS-81 Mir survey was a possible leak in the Spektr radiator. The discolored area has been very small in previous missions, hence it was not detected. The discolored area has increased in size since STS-79 and was measured to be approximately 7 sq. cm. in size during STS-81. The increased resolution of the new 400 mm lens on the 35 mm camera was instrumental in identifying this possible leak.

A second anomaly identified from the STS-81 imagery was charring and probable burn-throughs in the cable harness of the Igla antenna cable on Kristall. Additional features of peeling paint, discolorations of surfaces, and damage to solar arrays were also identified.

The STS-81 crew observed an apparent yaw of the Shuttle relative to Mir during docking. Analyses of the ODS centerline camera video showed the centerline camera to be misaligned in position and rotation with respect to the ODS, which may account for the apparent yaw. Video was also used to determine the indicated roll of the centerline and non-axial cameras during docking and pre-separation. These results are being evaluated by the JSC Structures and Mechanics Division.

Peeling paint is observed on the surfaces of the Spektr radiator, Base Block module, and the RSA carrier. The STS-81 imagery showed additional paint being peeled away from the Spektr radiator since STS-79. Also, additional paint has peeled (curled) on the upper part of the RSA carrier since its last imagery on STS-76. The imagery shows the existence of characteristic differences in the peeling paint processes of Spektr and the RSA carrier.

New features for which imagery was obtained were the Kurs antenna attached to the Docking Module and a power cable on the Base Block. First time coverage was obtained of the Mir-facing sides of the MEEP panels.

Imagery acquired with the 35 mm and 70 mm cameras provided excellent overview and detailed coverage of visible Mir surfaces throughout the mission. Imagery was obtained from the Shuttle, Spacehab, Base Block and Kvant-2 windows during the docked phase. Photography acquired during the fly-around with the 400 mm lens provided excellent overview coverage of the +XB, +YB, and -YB sides of Mir which are not seen during the docked phase. The new 400 mm lens on the 35 mm camera provided detailed information not obtained in previous mission imagery. This increased detail allowed more definitive analyses to be performed and additional information to be extracted on the condition of Mir.

The four PLB cameras were used in INCO-controlled acquisition of complementary Mir survey video imagery during crew sleep periods. This video imagery provided good coverage of the Shuttle-facing sides of the Spektr, Kvant-2, Base Block, Kristall, and Kvant modules. Imagery was also obtained of the Soyuz vehicle. Some video data was acquired of the Priroda. In addition, systematic coverage of the Docking Module and the attached RSA carrier was obtained.

Close-up still photographs were taken of the docking mechanism during both approach and backaway. These images were the highest quality obtained to date of this docking mechanism and did not show any anomalies of the docking mechanism. However, discoloration was noted on the non-axial target and traces of discoloration appeared adjacent to the structural latches. The discoloration of the non-axial target is also visible in

imagery taken during earlier phases of approach. The close-up imagery allowed detailed analyses of the docking mechanism which could not be performed with the video.

No unusual motion of Mir appendages was noted during the approach, docked, backaway, and fly-around phases of the Shuttle during the STS-81 mission.

11.2 Conclusions

Based on the summary of major points made above, the following conclusions have been made:

The imagery from the STS-81 mission substantially augmented the imagery from previous Shuttle/Mir missions. The combined imagery gathered on STS-63, 71, 74, 76, 79 and 81 missions provide significant information from which an assessment can be made about the effects of the space environment on an orbiting platform.

The imagery surveys continue to provide new information on the effects of the space environment on the Mir Space Station. These effects are observed on newly-deployed structures as well as on those structures and surfaces which have been on-orbit for years. Moreover, a time-history of imagery is being accumulated.

The amount of high-resolution imagery is increasing with each additional mission. This increase is allowing the identification of smaller features and improved definition of surface characteristics, including discoloration, micrometeoroid/orbital debris damage, and surface and structural anomalies.

The extent of observed discoloration of surfaces continues to spread. These observations are partially due to the continued collection of improved imagery. Recently-deployed surfaces also show discoloration. Characterizations of the sources of these discolorations are being investigated by environmental and materials engineers.

The 400 mm lens on the Nikon camera provides significantly improved resolution over the 300 mm lens and should be the large focal length lens of choice for Mir and International Space Station imagery surveys from the Shuttle. Use of the 400 mm focal length lens during the station-keep and fly-around provided improved coverage of Mir surfaces not visible during the docked phase. The 400 mm lens, in conjunction with the 180 mm lens and the Hasselblad with 100 and 250 mm lenses, provide a wide range of image acquisition capabilities.

11.3 Recommendations

Based on the summary above, crew comments during training and post-mission debriefs, and evaluation of the STS-81 and prior mission imagery, the following recommendations are made for upcoming missions:

- High resolution imagery of the Spektr radiator should continue to be acquired for each mission for purposes of monitoring the condition of the radiator.
- Acquisition of mission related timing is required for the video imagery to be correlated to mission related events. Synchronous timing should be a standard recording on the video. Crew time must also be allotted for set up of the video cameras prior to acquisition of planned structural dynamics tests. Set-up during daylight hours should be mandatory.
- The Nikon 35 mm camera with a 400 mm lens should be the primary photographic equipment for high-resolution survey imagery acquisition.

-
- Time stamps on the 35 mm film would have been a great support in analysis. A time stamp would allow correlation of the images with respective lenses and distances. The time-stamp option on the Nikon 35 mm F4 camera should be used as a standard procedure.
 - Centerline video camera views should be the primary source for determining the condition of the centerline docking target. However, for docking mechanism assessment, crew time should continue to be provided for acquisition of close-up film imagery. STS-81 imagery using the 35 mm camera with the 180 mm lens demonstrated the value of close-up imagery. Additional options for improving docking mechanism imagery include: improved lighting and vehicle orientation, changing the timelines for docking and backaway, improved imagery equipment, and station-keeping at close range after backaway.
 - If imagery is to be obtained of the Androgynous Peripheral Attachment System (APAS) electrical connectors, consideration should be given to using the 35 mm camera with the 400 mm lens during close approach and backaway in the range of 30 to 60 feet. The 180 mm lens was used during STS-81, however the 400 mm lens will double the resolution.
 - An updated mission-specific target priority list should continue to be generated for the crew. Configuration modifications and varying image acquisition requirements justify the need for an updated list for each mission.
 - INCO-controlled PLB video cameras should continue to be used to perform Mir surveys during crew sleep periods. This has been the most effective way to obtain survey video coverage and also allows real-time decisions to be made on target acquisition.
 - The need for bracketing exposures when acquiring imagery should continue to be emphasized. The bracketed exposures provide for additional detail in the imagery not obtained with a single exposure.
 - The crew should continue to be made aware of lighting conditions that highlight surface features. Lighting angles oblique to Mir surfaces convey textural information that would otherwise remain hidden.
 - At least one video camera should be imaging the Mir during fly-around. The Mir should fill the field-of-view of this video camera. Unanticipated array motion is easier to detect with this configuration.
 - Additional analyses of centerline camera alignment should be considered for previous and future docking missions.
 - The DTO-1118 experiences for imagery acquisition and analyses should be applied to the International Space Station program. Specific benefits arise from a continuum of imagery acquisition starting with on-orbit close-out imagery at each opportunity and periodic imagery surveys. Each viewing perspective (approach, docked, separation, fly-around) provides different types of information.

12. REFERENCES

NASA/RSC-E Joint Report, Mir Photo/TV Survey (DTO-1118): STS-63, JSC-27246, August 28, 1995.

NASA/RSC-E Joint Report, Mir Photo/TV Survey (DTO-1118): STS-71, JSC-27355 January 16, 1996.

NASA/RSC-E Joint Report, Mir Photo/TV Survey (DTO-1118): STS-74, JSC-27649, November 20, 1996.

Mir Photo/TV Survey (DTO-1118): STS-76 Mission Report JSC-27525, July 30, 1996.

Mir Photo/TV Survey (DTO-1118): STS-79 Mission Report JSC-27761, March 28, 1997.

13. ACRONYMS & ABBREVIATIONS

APAS	Androgynous Peripheral Attachment System
APDU	Androgynous Peripheral Docking Unit
CCD	Charge Coupled Device
CLTV	Centerline TV
CSA	Cooperative Solar Array
CTVC	Color Television Camera
DM	Docking Module
DTO	Detailed Test Objective
ESC	Electronic Still Camera
EVA	Extra Vehicular Activity
GMT	Greenwich Mean Time
HARR	Hemispherical Array Retroreflector
INCO	Instrumentation and Communication Officer
ITVC	Intensified TV Camera
IS&AG	Image Science & Analysis Group
ISS	International Space Station
JSC	Johnson Space Center
LMES	Lockheed Martin Engineering and Sciences
MEEP	Mir Environmental Effects Payload
MiSDE	Mir Structural Dynamics Experiment
MSRE	Mir Sample Return Experiment
NASA	National Aeronautics & Space Administration
ODC	Orbital Debris Collector
ODS	Orbiter Docking System
OSVS	Orbiter Space Vision System
PDA	Payload Disconnect Assembly
PLB	Payload Bay
PPMD	Polished Plate Micrometeoroid & Debris
POSA	Passive Optical Sample Assembly
POSA II	Passive Optical Sample Assembly II
ROEU	Remotely Operated Electrical Umbilical
RSA	Reusable Solar Array (same as MSA)
RSC-E	Russian Space Center-Energia
SA	Solar Array
SAR	Synthetic Aperture Radar
SP	Solar Panel
STS	Space Transportation System
TPS	Thermal Protection System
VRCS	Vernier Reaction Control System